



Modeling diurnal variation of surface PM_{2.5} concentrations over East China with WRF-Chem: impacts from boundary-layer mixing and anthropogenic emission

Qiuyan Du¹, Chun Zhao^{1,2}, Mingshuai Zhang¹, Xue Dong^{1,3}, Yu Chen¹, Zhen Liu⁴, Zhiyuan Hu^{5,6}, Qiang Zhang⁷, Yubin Li⁸, Renmin Yuan¹, and Shiguang Miao⁹

¹School of Earth and Space Sciences, University of Science and Technology of China, Hefei, 230026, China

²CAS Center for Excellence in Comparative Planetology, USTC, Hefei, 230026, China

³PowerChina Huadong Engineering Corporation Limited, Hangzhou, China

⁴School of Geosciences, University of Edinburgh, Edinburgh, UK

⁵School of Atmospheric Sciences and Guangdong Province Key Laboratory for Climate Change and Natural Disaster Studies, Sun Yat-sen University, Zhuhai, China

⁶Southern Marine Science and Engineering Guangdong Laboratory, Zhuhai, China

⁷Department of Earth System Science, Tsinghua University, Beijing, China

⁸School of Atmospheric Physics, Nanjing University of Information and Technology, Nanjing, China

⁹Institute of Urban Meteorology, Chinese Meteorology Administration, Beijing, China

Correspondence: Chun Zhao (chunzhao@ustc.edu.cn)

Received: 20 August 2019 – Discussion started: 27 September 2019

Revised: 7 January 2020 – Accepted: 6 February 2020 – Published: 6 March 2020

Abstract. Diurnal variation of surface PM_{2.5} concentration (diurnal PM_{2.5}) could dramatically affect aerosol radiative and health impacts and can also well reflect the physical and chemical mechanisms of air pollution formation and evolution. So far, diurnal PM_{2.5} and its modeling capability over East China have not been investigated and therefore are examined in this study. Based on the observations, the normalized diurnal amplitude of surface PM_{2.5} concentrations averaged over East China is weakest (~ 1.2) in winter and reaches ~ 1.5 in other seasons. The diurnal PM_{2.5} shows the peak concentration during the night in spring and fall and during the daytime in summer. The simulated diurnal PM_{2.5} with WRF-Chem and its contributions from multiple physical and chemical processes are examined in the four seasons. The simulated diurnal PM_{2.5} with WRF-Chem is primarily controlled by planetary boundary layer (PBL) mixing and emission variations and is significantly overestimated against the observation during the night. This modeling bias is likely primarily due to the inefficient PBL mixing of primary PM_{2.5} during the night. The simulated diurnal PM_{2.5} is sensitive to the PBL schemes and vertical-layer configurations with

WRF-Chem. Besides the PBL height, the PBL mixing coefficient is also found to be the critical factor determining the PBL mixing of pollutants in WRF-Chem. With reasonable PBL height, the increase in the lower limit of the PBL mixing coefficient during the night can significantly reduce the modeling biases in diurnal PM_{2.5} and also the mean concentrations, particularly in the major cities of East China. It can also reduce the modeling sensitivity to the PBL vertical-layer configurations. The diurnal variation and injection height of anthropogenic emissions also play roles in simulating diurnal PM_{2.5}, but the impact is relatively smaller than that from the PBL mixing. This study underscores that more efforts are needed to improve the boundary mixing process of pollutants in models with observations of PBL structure and mixing fluxes in addition to PBL height, in order to simulate reasonably the diurnal PM_{2.5} over East China. The diurnal variation and injection height of anthropogenic emissions must also be included to simulate the diurnal PM_{2.5} over East China.

1 Introduction

The Yangtze River delta (YRD) region of East China hosts the economic engine and a major portion of the Chinese population. During the past 2 decades, the rapid economic growth has resulted in significant elevated surface air pollutants over East China, especially particulate matter (PM), also called aerosols. Previous studies have indicated that exposure to the high concentrations of PM_{2.5} (fine particulate matter with aerodynamic diameters less than 2.5 µm) can cause many health issues such as lung cancer (LC), ischemic heart disease (IHD), asthma, and nervous system breakdown (e.g., Seaton et al., 1995; Davidson et al., 2005; Pope III and Dockery, 2006; Ho et al., 2018; Li et al., 2018; T. Liu et al., 2018). It has become the fourth risk factor of deaths in China, and 11.1 % of all deaths are attributable to the ambient elevated concentrations of particulate matter (GBD Risk Factors Collaborators, 2017). Besides the health impacts, atmospheric aerosols can also influence the radiative energy budget of the Earth's system by interacting with radiation, serving as cloud condensation nuclei (CCN) and ice nuclei (IN), and hence modifying cloud microphysics and precipitation (e.g., Ackerman, 1977; Dickerson et al., 1997; Jacobson, 1998; Li et al., 2009; Zhao et al., 2012).

Many studies have investigated spatial and temporal variations of atmospheric aerosol over China in the last decades. The PM_{2.5} concentrations are higher in North China than in South China. The highest surface PM_{2.5} concentrations appear in winter and the lowest in summer, and the highest and lowest surface PM_{2.5} concentrations of a day often occur in the evening and afternoon, respectively (e.g., Gong et al., 2007; Fu et al., 2008; Hu et al., 2014; Z. F. Wang et al., 2014; Y. G. Wang et al., 2014; Y. J. Wang et al., 2014; Chen et al., 2015; Geng et al., 2015; Li et al., 2015; Xie et al., 2015; Zhang and Cao, 2015; H. Zhang et al., 2015; Chen et al., 2016). Moreover, modeling analysis can help understand the chemical and physical processes affecting aerosol formation and evolution (e.g., Ying et al., 2009; Zhang et al., 2010; Liao et al., 2014; Y. X. Wang et al., 2014; Y. J. Wang et al., 2014; Cheng et al., 2016; Z. Hu et al., 2016; Li et al., 2016; Yang et al., 2016; J. Hu et al., 2016; Zhao et al., 2017). Yang et al. (2016) reproduced an increasing trend of winter PM_{2.5} concentrations averaged over East China for 1985–2005 with the GEOS-Chem model and found that the variations in anthropogenic emissions dominated the increase in winter surface PM_{2.5} concentrations over East China, and the variations in meteorological fields also played an important role in influencing the decadal increase in winter PM_{2.5} concentrations over East China. J. Hu et al. (2016) investigated the spatial and temporal distribution of secondary organic aerosol (SOA) in China in 2013 with the WRF-CMAQ model and found that the formation of SOA from biogenic emissions was significantly enhanced due to anthropogenic emissions.

Most of the previous modeling studies focused on understanding the mechanisms driving PM variation on daily or seasonal scales or/and evaluating the simulation of daily and monthly mean PM concentrations over East China. Few studies evaluated the model performance in simulating the diurnal cycle of surface PM concentrations and investigated the mechanisms underneath. However, the model capability of capturing the diurnal cycle of surface PM concentrations is critical for revealing mechanisms of PM formation and evolution and may also affect the simulation of mean concentrations. Some studies also found that diurnal variation of surface PM concentrations can affect the daily average radiative forcing (e.g., Arola et al., 2013; Kassianov et al., 2013; Kuang et al., 2015; Z. Wang et al., 2015; Song et al., 2018). Based on the ground-based data collected in Hefei from 2007 to 2013, Z. Wang et al. (2015) demonstrated that using daily averaged aerosol properties to retrieve the 24 h average direct aerosol radiative forcing can have positive biases of up to 7.5 W m⁻² for the cases. Arola et al. (2013) found that the aerosol optical depth (AOD) diurnal cycles have significant impacts on the daily mean aerosol radiative forcing.

Previous studies have observed evident diurnal variations of surface PM over East China (e.g., Gong et al., 2007; Gu et al., 2010; Pathak et al., 2011; Feng et al., 2014; Hu et al., 2014; Huang et al., 2014; Ma et al., 2014; Zhang and Cao, 2015; Chen et al., 2016, 2017; Tao et al., 2016; Zhao et al., 2016; Jia et al., 2017; H. Guo et al., 2017; J. Guo et al., 2017). Zhang and Cao (2015) used a long-term dataset of surface PM_{2.5} concentrations measured at 190 cities of China and found that the diurnal variation of the PM_{2.5}-to-CO ratio consistently displayed a pronounced peak during the afternoon, reflecting a significant contribution of secondary PM formation. H. Guo et al. (2017) investigated the diurnal cycle of PM_{2.5} in China with the observations obtained at 226 sites of China during the period of January of 2013 to December of 2015 and found that the surface PM_{2.5} concentrations reached the maximum in the morning over the YRD region.

Diurnal variation of surface PM concentrations can be controlled by many factors, including emissions, chemical reactions, and meteorology (e.g., Wang et al., 2006, 2010, 2016; Huang et al., 2010; Menut et al., 2012; Qi et al., 2012; Quan et al., 2013; Tiwari et al., 2013; Li et al., 2014; Pal et al., 2014; Sun et al., 2015; Tao et al., 2015; Zhang and Cao, 2015; Chen et al., 2016; Roig Rodelas et al., 2019; Xu et al., 2019). Wang et al. (2010) found that simulations with an hourly emission inventory can reproduce the diurnal variation patterns and magnitudes of AOD better than simulations with a daily emission inventory. Xu et al. (2019) compared the diurnal cycles of aerosol species between 2014 and 2016 observed by an Aerodyne high-resolution aerosol mass spectrometer in Beijing and found that the increases in secondary inorganic nitrate, sulfate, and ammonium throughout the day in 2016 were mainly caused by the enhanced photochemical production. With the dataset of PBL height derived from the space-borne and ground-based lidar, Su et al. (2018) in-

vestigated the relationship between PBL height and surface PM concentrations across China and found nonlinearly negative responses of PM to PBL height evolution over polluted regions, especially when the PBL height is shallow and the PM concentration is high.

Since very few studies evaluated the modeling performance of the diurnal cycle of surface PM concentrations over East China and investigated the mechanisms underneath, this study investigates the WRF-Chem (Weather Research and Forecasting model coupled with Chemistry) simulation of the diurnal variation of PM_{2.5} over East China. WRF-Chem (Grell et al., 2005; Skamarock et al., 2008; Powers et al., 2017) is an online-coupled meteorology and chemistry model that simulates meteorological fields and air pollutant concentrations simultaneously. It has been widely used for studying the temporal and spatial variation of aerosols (e.g., Jiang et al., 2012; Zhou et al., 2014, 2017; Bei et al., 2016; Wang et al., 2016; Zhang et al., 2016; Zhong et al., 2016; P. Li et al., 2017; Zhao et al., 2017; S. Liu et al., 2018; Ni et al., 2018) and their meteorological and climatic impacts over East China (e.g., Gong et al., 2007; Ding et al., 2013; Wu et al., 2013; Gao et al., 2014; Chen et al., 2014; Zhao et al., 2014; B. Zhang et al., 2015; L. Zhang et al., 2015; Huang et al., 2016; Liu et al., 2016; Petäjä et al., 2016; B. Zhao et al., 2017). Most of the previous modeling studies with WRF-Chem over China investigated the influencing factors on spatial distribution and monthly or seasonal variation of PM. None of them focused on the performance of simulating the diurnal variation of PM with WRF-Chem.

The study will examine the observed characteristics of diurnal variation of surface PM_{2.5} concentrations over the YRD region of East China in four seasons of 2018. The WRF-Chem simulations are conducted for 1 month of each season over East China as shown in Fig. 1a, and the simulated diurnal cycle of surface PM_{2.5} concentrations will be evaluated by comparing with hourly observations of surface PM_{2.5} concentrations released by the Ministry of Environmental Protection (MEP) of China for 190 stations over the YRD region of East China in 2018. The model is also used to investigate the mechanisms driving the diurnal cycle of surface PM_{2.5}. This study will focus on the impacts from meteorology and anthropogenic emissions on the diurnal variation of surface PM_{2.5} concentrations. For meteorology, we will focus on the PBL mixing process that has been found to largely control the diurnal variation of surface pollutant concentrations (M. Liu et al., 2018). For emissions, based on the findings of Wang et al. (2010) and Yang et al. (2019), the diurnal variation and injection height of emission will be investigated. The rest of the paper is organized as follows. The detailed introduction of WRF-Chem model and numerical experiments, anthropogenic emissions, and observations will be presented in Sect. 2. The examination of the simulated diurnal variation of surface PM_{2.5} concentrations and the impacts of PBL mixing and emission will be discussed in

Sect. 3. The summary and discussion can be found in Sects. 4 and 5, respectively.

2 Methodology

2.1 Models and experiments

2.1.1 WRF-Chem

In this study, the version of WRF-Chem updated by the University of Science and Technology of China (USTC version of WRF-Chem) is used. This USTC version of WRF-Chem includes some additional capabilities such as the diagnosis of radiative forcing of aerosol species, land surface coupled biogenic VOC (volatile organic compound) emission, and aerosol–snow interaction compared with the publicly released version (Zhao et al., 2013a, b, 2014, 2016; Hu et al., 2019). Particularly, in order to understand the modeling mechanisms driving the diurnal variations of surface PM_{2.5} concentrations over East China, this study updates the USTC version of WRF-Chem to include the diagnosis of contributions to surface PM_{2.5} concentrations from individual processes, including transport, emission, dry and wet deposition, PBL mixing, and chemical production/loss, by estimating the difference of surface PM_{2.5} concentrations before and after individual processes during the simulation. More specifically, the contribution of each process is estimated in the following formula:

$$CT_{P,S,T} = C_{P,S,T} - C_{P,S,T_0}, \quad (1)$$

where C_{P,S,T_0} and $C_{P,S,T}$ represent the concentration of species S before (model time T_0) and after (model time T), respectively, the process P . Therefore, $CT_{P,S,T}$ represents the contribution of the process P to the change in concentration of species S during the time period $(T - T_0)$. For example, if C_0 and C represent the surface concentrations of PM_{2.5} before (T_0) and after (T), respectively, the PBL mixing, the contribution (CT) of PBL mixing to the change in surface concentrations of PM_{2.5} during the time period $(T - T_0)$ can be estimated as $(C - C_0)$. The overall contribution during a specific time period (e.g., 1 d) can be obtained by integrating $CT_{P,S,T}$ for this time period.

The Model for Simulating Aerosol Interactions and Chemistry (MOSAIC, Zaveri and Peters, 1999; Zaveri et al., 2008) and the CBM-Z (carbon bond mechanism) photochemical mechanism (Zaveri and Peters, 1999) are used. The MOSAIC aerosol scheme includes physical and chemical processes of nucleation, condensation, coagulation, aqueous-phase chemistry, and water uptake by aerosols. All major aerosol components including sulfate, nitrate, ammonium, black carbon (BC), organic matter (OM), sea salt, mineral dust, and other inorganics (OIN) are simulated in the model. OIN represents the unidentified aerosol species other than OM, BC, sulfate, ammonium, and nitrate in emissions if

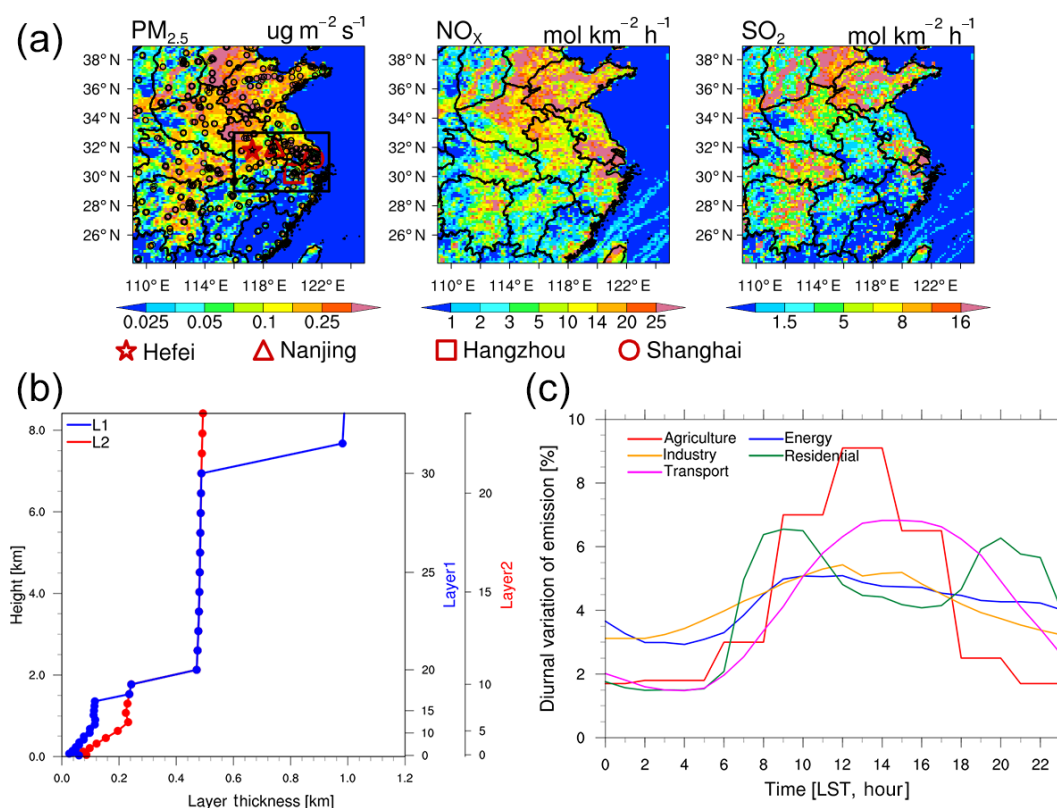


Figure 1. (a) Emissions of SO₂, NO₂, and PM_{2.5} from the MEIC China inventory over the simulation domain (109.0–124.9° E, 24.0–38.9° N) with black boxes showing the analyzed domain (116.0–122.5° E, 29.0–33.0° N), overlaid with observational sites and four cities as the center (Shanghai, 121.45° E and 31.21° N) and sub-center (Nanjing, 118.78° E and 32.06° N; Hefei, 117.25° E and 31.85° N; Hangzhou, 120.08° E and 30.21° N) of the YRD city cluster. (b) Vertical profiles of the layer thickness from L1 and L2 layer configuration. (c) Diurnal profiles of emissions from five individual sectors (agriculture, industry, transport, energy, and residential).

any, which are composed mostly of minerals in emissions in this study. Aerosol size distributions are represented by eight discrete size bins through the bin approach (Fast et al., 2006). Dry deposition of aerosol mass and number is simulated following the approach of Binkowski and Shankar (1995), which includes both particle diffusion and gravitational effects. Wet removal of aerosols by grid-resolved stratiform clouds/precipitation includes in-cloud removal (rainout) and below-cloud removal (washout) by impaction and interception, following Easter et al. (2004) and Chapman et al. (2008). In this study, cloud-ice-borne aerosols are not explicitly treated in the model, but the removal of aerosols by the droplet freezing process is considered. Convective transport and wet removal of aerosols by cumulus clouds follow Zhao et al. (2013a). Aerosol radiative feedback is coupled with the Rapid Radiative Transfer Model (RRTMG) (Mlawer et al., 1997; Iacono et al., 2000) for both SW (shortwave) and LW (longwave) radiation as implemented by Zhao et al. (2011). The optical properties and direct radiative forcing of individual aerosol species in the atmosphere are diagnosed following the methodology described in Zhao et al. (2013b). A detailed description of the computation of aerosol optical

properties in WRF-Chem can be found in Fast et al. (2006) and Barnard et al. (2010). Aerosol–cloud interactions were included in the model by Gustafson et al. (2007) for calculating the activation and re-suspension between dry aerosols and cloud droplets.

2.1.2 Numerical experiments

In this study, WRF-Chem is conducted with two nested domains (one-way nesting) in 1 month of each season of 2018 (i.e., January, April, July, and October of 2018). The outer quasi-global domain with 360 × 145 grid cells (180° W–180° E, 67.5° S–77.5° N) at the 1° × 1° horizontal resolution is used to provide the chemical boundary to the inner domain with 112 × 105 grid cells (109.0–124.9° E, 24.0–38.9° N) at the horizontal resolution of 15 km over East China covering the entire YRD region as shown in Fig. 1a. More details about the quasi-global WRF-Chem simulation can be found in Zhao et al. (2013a) and Z. Hu et al. (2016). To better resolve the PBL structure and mixing and examine the modeling sensitivity to vertical configuration within the PBL, two experiments (CTL1 and CTL2, Table 1) are configured with 40 vertical layers, but have different distributions (as shown

Fig. 1b). One configuration (L1) has roughly 20 layers below 2 km above the ground, and the other has about 10 layers below 2 km (Fig. 1b). In both CTL1 and CTL2, the MYNN2 PBL scheme (Nakanishi and Niino, 2006) is used. To demonstrate the modeling sensitivity to PBL parameterizations, experiment CTL3 is conducted in a way similarly to CTL2 but with the YSU PBL scheme (Hong et al., 2006). Since this study focuses on understanding the PBL mixing impact, the calculation of the PBL mixing coefficient within the MYNN2 and YSU PBL schemes is briefly described here. In local closure PBL scheme MYNN, the PBL mixing coefficient is calculated following Mellor and Yamada (1982):

$$K_{h,m} = lqS_{h,m}, \quad (2)$$

where l is the mixing-length scale, S_h and S_m are stability functions, and q is related to the turbulent kinetic energy (TKE) in the following formula:

$$q = (2 \cdot \text{TKE})^{1/2}. \quad (3)$$

In the non-local closure PBL scheme YSU, the momentum mixing coefficient K_m is formulated following Hong et al. (2006):

$$K_m = kw_s z \left(1 - \frac{z}{h}\right)^p, \quad (4)$$

where p is the profile shape exponent taken to be 2, k is the von Karman constant, z is the height from the surface, and h is PBL height. For the eddy mixing coefficient for temperature and moisture K_h can be estimated from K_m with the relationship of the Prandtl number as in Noh et al. (2003):

$$Pr = K_m/K_h, \quad (5)$$

$$Pr = 1 + (Pr_0 - 1) \exp \left[\frac{-3(z - \varepsilon h)^2}{h^2} \right]. \quad (6)$$

Two additional sensitivity experiments (EXP1 and EXP2, Table 1) are also conducted corresponding to experiments CTL1 and CTL2, respectively, except that the PBL mixing coefficient is modified (see details in Sect. 3.2.2).

All these WRF-Chem experiments use the Morrison two-moment cloud microphysics (Morrison et al., 2009), Kain–Fritsch convective scheme (Kain, 2004), CLM land surface scheme, and RRTMG longwave and shortwave radiation schemes. The meteorological initial and lateral boundary conditions are derived from the NCEP Final reanalysis data with $1^\circ \times 1^\circ$ resolution and 6 h temporal resolution. The modeled u component and v component wind and atmospheric temperature are nudged towards the reanalysis data only to the layers above the PBL with nudging coefficients of $3 \times 10^{-4} \text{ s}^{-1}$ with a nudging timescale of 6 h (Stauffer and Seaman, 1990; Seaman et al., 1995).

2.1.3 Emissions

Anthropogenic emissions for the outer quasi-global simulation are obtained from the Hemispheric Transport of Air

Pollution version-2 (HTAPv2) at $0.1^\circ \times 0.1^\circ$ horizontal resolution and a monthly temporal resolution for year 2010 (Janssens-Maenhout et al., 2015), except that emissions over China within the domains are from the Multi-resolution Emission Inventory for China (MEIC) at $0.1^\circ \times 0.1^\circ$ horizontal resolution for 2015 (Li et al., 2017a, b), which is also used for the inner domain simulation over East China. Figure 1a shows the spatial distributions of emissions of primary PM_{2.5}, NO_x, and SO₂ over East China. The default anthropogenic emission inventories assume no diurnal variation of emissions and that all emissions are near the surface (e.g., the first model layer). Since diurnal variation of emissions and injection height of power plant emissions may have impacts on the diurnal variation of surface pollutants, the experiments discussed above apply the diurnal profiles of anthropogenic emissions from five individual sectors (i.e., agriculture, industry, transport, energy, and residential) following X. Wang et al. (2010) and Wang et al. (2005) as shown in Fig. 1c and vertical distributions of anthropogenic power plant emissions following Wang et al. (2010) as shown in Table 2. Wang et al. (2010) derived the vertical profiles for East Asia based on the dataset of the US and found that the profiles are comparable to those estimated in China and Japan (Woo et al., 2003; Wang et al., 2010). As shown in Fig. 1c, emissions from all sectors show peak values during the daytime, and the diurnal variations from agriculture, residential, and transportation are much stronger than those from industry and power plants. The emissions from power plants are distributed from the bottom to a height of ~ 900 m, with more than 90 % below 500 m. Both diurnal and vertical variation profiles of anthropogenic emissions are prescribed without temporal variability. Two sensitivity experiments, EXP1_E1 and EXP1_E2, are conducted similarly to EXP1, except that EXP1_E1 assumes no diurnal variation of anthropogenic emissions and EXP1_E2 assumes all power plant emissions are placed near the surface (i.e., the first model layer). Comparing EXP1 with EXP1_E1 and EXP1_E2 can examine the impact of diurnal variation and injection height of anthropogenic emissions on the diurnal cycle of surface PM_{2.5}, respectively. All these experiments are summarized in Table 1. Biomass burning emissions are obtained from the Fire Inventory from NCAR (FINN) with hourly temporal resolution and 1 km horizontal resolution (Wiedinmyer et al., 2011). The biomass burning emissions follow the diurnal variation provided by WRAP (2005) and the injection heights suggested by Dentener et al. (2006) from the Aerosol Comparison between Observations and Models (AeroCom) project. Sea-salt emission follows Zhao et al. (2013a), which includes correction of particles with radii less than $0.2 \mu\text{m}$ (Gong, 2003) and dependence of sea-salt emission on sea surface temperature (Jaeglé et al., 2011). The vertical dust fluxes are calculated with the GOCART dust emission scheme (Ginoux et al., 2001), and the emitted dust particles are distributed into the MOSAIC aerosol size bins following a theoretical expression based on the physics of scale-invariant fragmentation of brittle materi-

Table 1. Numerical experiments conducted in this study.

Name	PBL scheme	Vertical structure	PBL mixing coefficient (m ² s ⁻¹)	Emission diurnal cycle	Emission injection height
CTL1	MYNN	layer1	Minimum = 0.1	Yes	Yes
CTL2	MYNN	layer2	Minimum = 0.1	Yes	Yes
CTL3	YSU	layer2	Minimum = 0.1	Yes	Yes
EXP1	MYNN	layer1	Minimum = 5.0	Yes	Yes
EXP2	MYNN	layer2	Minimum = 5.0	Yes	Yes
EXP1_E1	MYNN	layer1	Minimum = 5.0	No	Yes
EXP1_E2	MYNN	layer1	Minimum = 5.0	Yes	No

Table 2. Vertical distributions of power plant emissions: percentage of each species allocated to the height of the vertical layers in the WRF-Chem model.

Species	Height of emission layers (m)				
	0–76	76–153	153–308	308–547	547–871
SO ₂	5 %	30 %	35 %	25 %	5 %
NO _x	5 %	40 %	25 %	25 %	5 %
CO	5 %	70 %	20 %	5 %	0 %
NH ₃	5 %	75 %	15 %	5 %	0 %
NMVOC	5 %	85 %	10 %	0 %	0 %
PM _{2.5}	5 %	45 %	25 %	20 %	5 %
PM ₁₀	5 %	55 %	20 %	15 %	5 %
OC	5 %	70 %	15 %	10 %	0 %
BC	5 %	65 %	20 %	10 %	0 %

als derived by Kok (2011). More details about the dust emission scheme coupled with the MOSAIC aerosol scheme in WRF-Chem can be found in Zhao et al. (2010, 2013a).

2.2 Observations

The ground observations of hourly surface PM_{2.5} mass concentrations in January, April, July, and October of 2018 are obtained from the website of the Ministry of Environmental Protection of China (MEP of China). Since this study focuses on the YRD region of East China, 190 stations over East China are selected for analysis. The locations of these 190 stations are shown in Fig. 1a within the black box (116.0–122.5° E, 29.0–33.0° N). Besides regional average analysis, four cities (Fig. 1a) as the center (Shanghai, 121.45° E and 31.21° N) and sub-center (Nanjing, 118.78° E and 32.06° N; Hefei, 117.25° E and 31.85° N; Hangzhou, 120.08° E and 30.21° N) of the YRD city cluster are also selected for further analysis in urban areas.

3 Results

3.1 Modeling diurnal cycle of surface PM_{2.5} concentration

In order to investigate the diurnal cycle of surface PM_{2.5} concentrations, this study defines an index to better show the diurnal variation. The diurnal index (DI) is defined as the value of each hour divided by the minimum value within 24 h on monthly average. The peak DI within 24 h represents the amplitude of diurnal variation. Figure 2 shows the diurnal index of surface PM_{2.5} concentrations within 24 h averaged over the YRD region of East China (as shown in the black box in Fig. 1a) for January, April, July, and October of 2018 from the WRF-Chem experiments and observations. Experiment CTL1 uses the MYNN PBL scheme and a finer boundary-layer configuration (L1 in Fig. 1b). The simulation results and the observations are sampled 3-hourly at the observational sites as shown in Fig. 1a. On regional average, the observed variation of DI is weakest in winter, with the peak value around 1.2 among the four seasons. The observed DI reaches the maximum of 1.5 in autumn. In spring and autumn, the observed diurnal variations of DI are similar, showing the peak during the night and reaching the minimum in the afternoon, which is consistent with previous findings with observations over East China (e.g., Zhang and Cao, 2015; Liu et al., 2016; Guo et al., 2017). In summer, different from other seasons, the observed diurnal variation of DI shows the single peak around 1.4 near noontime. The CTL1 experiment can generally reproduce the peak during the night; however, the CTL1 simulation overestimates the observed peak DI in the two seasons, particularly in autumn. The experiment generally captures the seasonality of DI of surface PM_{2.5} concentrations, that is, the higher DI in spring and autumn and the weakest DI in winter, except that in summer the experiment significantly overestimates the DI during the night and produces an opposite diurnal pattern with the minimum DI near noontime. The spatial distributions of DI over East China are also generally consistent between observations and simulations and show similar seasonality (Fig. S1 in the Supplement). The area with higher surface PM_{2.5} con-

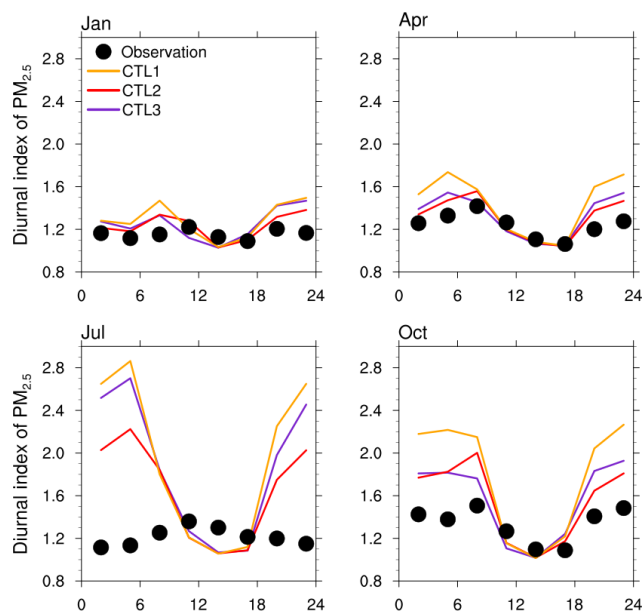


Figure 2. Diurnal index of surface PM_{2.5} concentrations within 24 h averaged over the YRD region of East China (within the black box of Fig. 1a) for January, April, July, and October of 2018 from experiments CTL1, CTL2, and CTL3, and observations. Both the simulated results and observations are sampled at the model output frequency, i.e., 3-hourly.

centrations generally has a higher DI (Fig. S2), particularly from the simulation.

Therefore, the DI distributions at the four cities as the center (Shanghai) and sub-center (Nanjing, Hefei, Hangzhou) of the YRD city cluster in East China (as shown in Fig. 1a) are further analyzed. Figure 3 shows the diurnal index of surface PM_{2.5} concentrations within 24 h averaged over the four cities for January, April, July, and October of 2018 from the WRF-Chem experiments and observations. The observed diurnal variations of DI in these four cities are consistent with that on the regional average of East China. The diurnal variations of DI are more evident in the two inland cities (Hefei and Nanjing) than the two coastal cities (Hangzhou and Shanghai). Consistent with the results based on the regional average, the CTL1 experiment can generally capture the diurnal variation of the DI of surface PM_{2.5} in the four cities, but overestimates the DI in the night, particularly in spring and autumn. In summer, again, CTL1 significantly overestimates the DI during the night and produces the opposite diurnal pattern compared to observations. In general, CTL1 produces even higher DI during the night in the four cities than the regional average, which results in larger diurnal amplitudes in the four cities than the regional average. CTL1 can generally simulate stronger diurnal variation in the two inland cities than in the two coastal cities.

The analysis above for both regional average and city average indicates that the CTL1 simulation has high positive bi-

ases of DI during the night. In order to understand the modeling biases and the mechanisms driving the simulated diurnal variations of surface PM_{2.5} concentrations over East China, the contribution to the diurnal variation of surface PM_{2.5} concentrations from individual processes, including transport, emission, dry and wet deposition, mixing, and chemical production/loss, is estimated. The contribution is calculated as the difference of surface PM_{2.5} concentrations before and after individual processes during the simulation. Figure 4 shows the contribution of individual processes to the variation of surface PM_{2.5} concentrations every 3 h in Hefei from the WRF-Chem experiments averaged for January, April, July, and October of 2018. The 3-hourly tendency (the difference between the current time and the time 3 h earlier) of surface PM_{2.5} concentrations is also shown. The contributions and tendencies are divided by monthly mean surface PM_{2.5} concentrations for each month. The results for the other three cities (Nanjing, Hangzhou, Shanghai) are similar to that of Hefei and are shown in Fig. S3a–c. Process contribution analysis is verified by comparing the variations of surface PM_{2.5} concentrations with the sum of the contributions from each individual process. As shown in Fig. S4, the sum contributions of all processes are consistent with the variations in surface PM_{2.5} concentrations following the principle of mass balance.

In Fig. 4, a positive value denotes a relative increase in surface PM_{2.5} concentrations and a negative value denotes a relative decrease. From the CTL1 experiment, the contributions from emission and chemistry are positive through the day, while the contributions from transport, PBL mixing, and wet and dry deposition are negative through the day. CTL1 simulates the largest variation of tendency in summer and the smallest variation in winter. The tendencies are negative from the morning to the afternoon, resulting in the simulated minimum surface PM_{2.5} concentrations in the afternoon in all seasons, which is consistent with the result shown in Fig. 3. It is evident that emission, PBL mixing, and transport are the three main processes controlling the diurnal variation of surface PM_{2.5} concentrations, and emission and PBL mixing are the dominant two. Emission increases the surface PM_{2.5} concentrations and reaches the maximum near noontime, while PBL mixing reduces the surface PM_{2.5} concentrations and also reaches the maximum reduction near noontime. The combined effect of emission and PBL mixing is reflected as the overall tendency. Therefore, PBL mixing is the determinant process leading to the simulated minimum DI near noontime and higher DI during the night. To further demonstrate the contribution of each PM_{2.5} composition to the diurnal variation of surface PM_{2.5} concentrations, Fig. 5 shows the diurnal variation of surface concentration of each PM_{2.5} composition in Hefei from the WRF-Chem experiments averaged for January, April, July, and October of 2018. The diurnal variations of surface concentrations of OM, BC, and OIN are larger than other components of PM_{2.5}, showing evident higher concentrations during the night and minimum

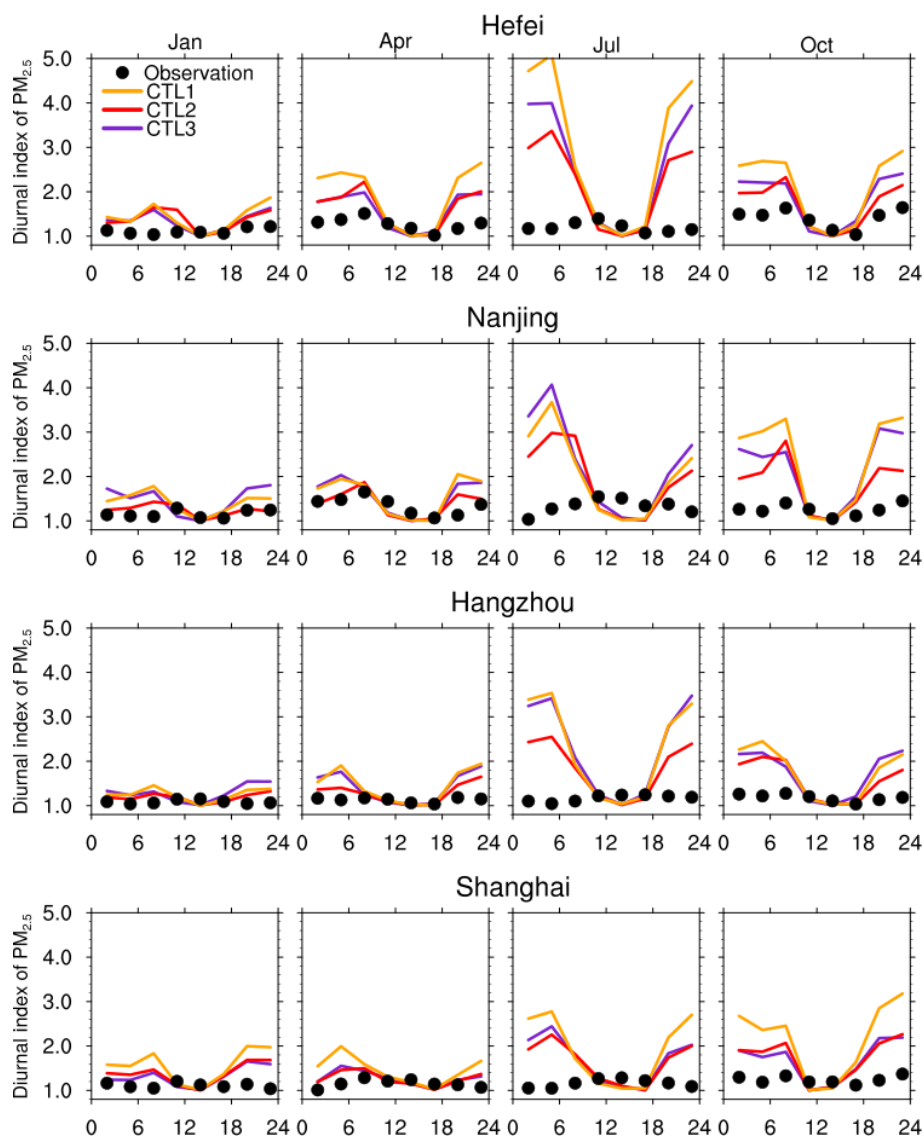


Figure 3. Diurnal index of surface PM_{2.5} concentrations within 24 h averaged over four cities (Hefei, Nanjing, Hangzhou, Shanghai) for January, April, July, and October of 2018 from experiments CTL1, CTL2, and CTL3, and observations.

near noontime in all seasons except winter. The sum of OM and OIN contributes to more than half of surface PM_{2.5} concentrations. Therefore, it suggests that the PBL mixing of the primary PM_{2.5} determines the simulated diurnal variation of surface PM_{2.5} concentrations. The results for the other three cities (Nanjing, Hangzhou, Shanghai) are similar to that of Hefei and are shown in Fig. S5a–c.

In order to understand the possible reasons for these modeling biases, some basic meteorological fields are evaluated with available observations. Since the modeled winds at the layers above the PBL are nudged towards the reanalysis data, the large-scale circulation can be well simulated. The winds at 850 hPa for each season are compared with the NCEP Final reanalysis dataset (FNL) and ERA5 reanalysis dataset (<https://rda.ucar.edu/datasets/ds630.0/>, last ac-

cess: 28 December 2019) (Fig. S6). The simulated wind circulation is highly correlated with the two reanalysis datasets with the spatial correlation coefficients of 0.9–0.97 over East China. The simulated temperature at 2 m is also evaluated with the available observations by the China Meteorological Administration (CMA) at the stations of East China (Figs. S7 and S8). The model captures the diurnal variation of near-surface temperature very well over East China. For near-surface winds, although the model generally overestimates the observed values by less than 10 %, the simulated diurnal variation is generally consistent with the observations over East China (Figs. S9 and S10). As the evaluation shows, the basic meteorological fields are generally simulated reasonably. The characteristics associated with the PBL mixing are further investigated below.

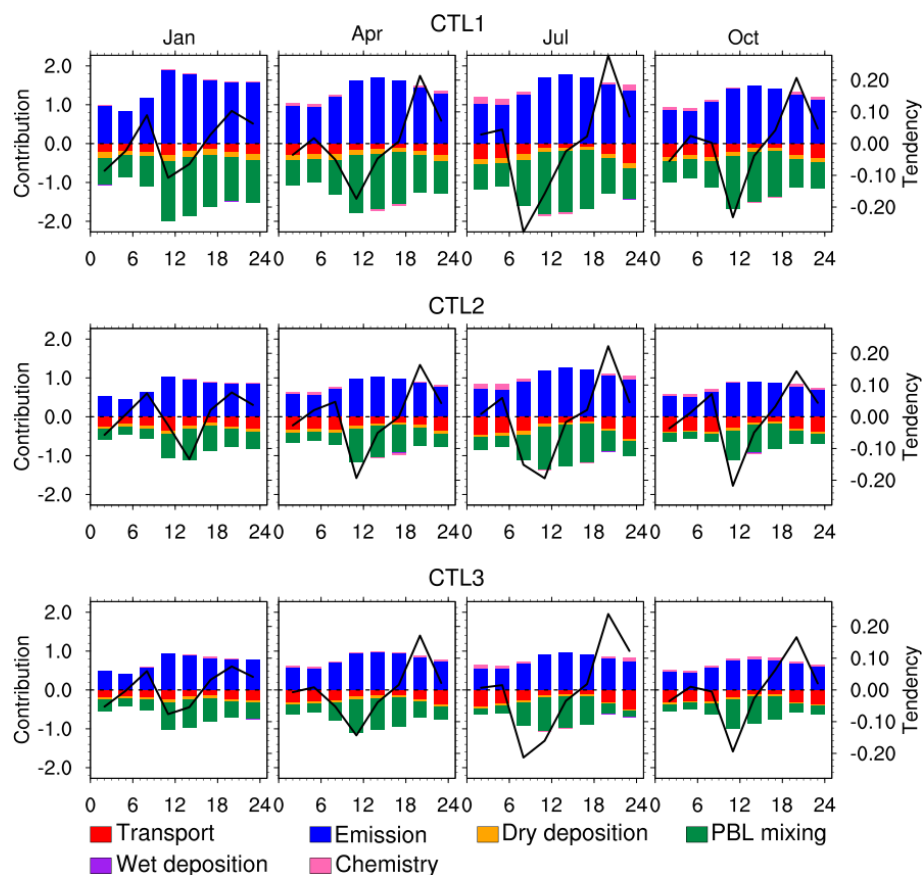


Figure 4. Relative contribution (normalized by monthly mean surface PM_{2.5} concentrations for each month) to surface PM_{2.5} concentrations every 3 h from individual process (transport, emission, dry and wet deposition, PBL mixing, chemical production/loss) averaged over Hefei for January, April, July, and October of 2018 from experiments CTL1, CTL2, and CTL3. The 3-hourly relative tendency of surface PM_{2.5} concentrations is also shown as the black line.

3.2 Sensitivity to PBL mixing

3.2.1 Sensitivity to the PBL configuration

As discussed above, the PBL mixing is very important for modeling diurnal variation of surface PM_{2.5} concentrations, and it may be affected by PBL parameterizations and vertical layer configurations within the PBL. Therefore, two experiments, CTL2 and CTL3, are conducted to examine the sensitivity of simulated diurnal variation of surface PM_{2.5} concentrations to different PBL configurations. CTL2 uses the same MYNN PBL scheme as CTL1 but is configured with a different vertical-layer distribution (L2) as shown in Fig. 1b, in which fewer vertical layers are put within the PBL as described in Sect. 2.2. CTL3 uses the YSU PBL scheme and is configured with the same L2 vertical layer distribution as CTL2. As shown in Fig. 2, on regional average, CTL2 and CTL3 generally simulate similar diurnal and seasonal patterns to that by CTL1, with the minimum DI near noontime and the peak DI during the night. CTL2 simulates lower DI than CTL1 during the night in all seasons. This indicates that

the model with a finer vertical resolution within the PBL, which is supposed to better resolve the PBL structure, produces higher positive biases of DI. CTL3 simulates similar diurnal variation of DI to CTL2 but overestimates the DI during the night to some extent, particularly in summer, which indicates the model with the YSU PBL scheme produces higher positive biases of DI during the night compared to the one with the MYNN PBL scheme. In the four cities as shown in Fig. 3, CTL2 and CTL3 also simulate similar diurnal and seasonal patterns to that by CTL1. It is also interesting to note that the difference of DI between CTL2 and CTL1 is larger than that between CTL3 and CTL2, which indicates that the modeling sensitivity of DI to the vertical-layer configurations within the PBL is even greater than that to the PBL schemes. Overall, all three of these WRF-Chem experiments produce similar positive biases of DI during the night compared to the observations in all seasons over the YRD region of East China, particularly in cities. This is consistent with previous findings about the simulated positive biases of diurnal variation of surface PM_{2.5} concentrations over East China (e.g., M. Liu et al., 2018). M. Liu et al. (2018) found that the

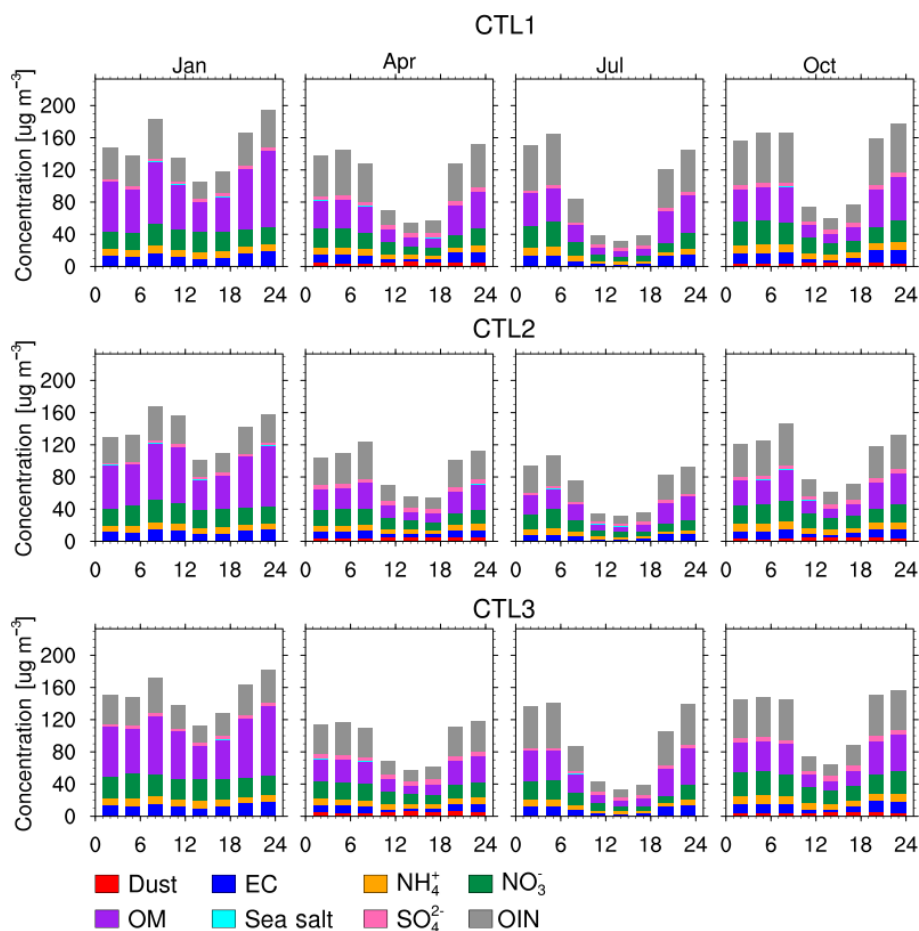


Figure 5. Diurnal variation of surface concentrations of each PM_{2.5} composition (dust, OM, EC, sea salt, NH₄⁺, SO₄²⁻, NO₃⁻, and other inorganics) averaged over Hefei for January, April, July, and October of 2018 from experiments CTL1, CTL2, and CTL3.

air quality model (WRF-CMAQ v5.0.1) also overestimated the surface concentrations of PM_{2.5} during the nighttime in October–December 2013. They speculated that the overestimation is due to the weak PBL mixing in the nighttime and claimed that the newer version of CMAQ v5.1 driven by WRF v3.7 revised the PBL mixing scheme (ACM2) and might reduce the nighttime biases. To verify this, two experiments are conducted using the ACM2 PBL scheme with WRF-Chem v3.5 and WRF-Chem v4.0, respectively, over East China for October of 2018. The results showed that the PBL mixing of the ACM2 scheme is enhanced in v4.0 compared to v3.5, especially during the night, and the simulated nighttime surface PM_{2.5} concentrations are reduced to some extent in v4.0 compared to v3.5 (not shown). However, the simulation still significantly overestimates the surface PM_{2.5} concentrations during the night. Therefore, the changes in PBL schemes and vertical configurations within the PBL can affect the simulated DI but cannot improve the simulations to reproduce the observations.

In order to better understand the modeling sensitivity of DI to the PBL configuration, Figs. 4 and 5 also show the simu-

lated results for the city of Hefei from CTL2 and CTL3. Similarly to CTL1, the results from CTL2 and CTL3 also show that emission, PBL mixing, and transport are the three main processes controlling the diurnal variation of surface PM_{2.5} concentrations, and emission and PBL mixing are the dominant two (Fig. 4). Since the number of vertical layers within the PBL in CTL2 and CTL3 is much less than that in CTL1, the thickness of the first model layer in CTL2 and CTL3 is about a factor 2 of that in CTL1. With the same emission flux, CTL2 and CTL3 simulate much smaller contributions from emissions to the surface PM_{2.5} concentrations than does CTL1. Correspondingly, the contributions from PBL mixing to the surface PM_{2.5} concentrations in CTL2 and CTL3 are also lower than that in CTL1. The combined effect of emission and PBL mixing results in weaker diurnal variation of surface PM_{2.5} concentrations in CTL2 and CTL3 than that in CTL1, as shown by the diurnal variation of the overall tendency of surface PM_{2.5} concentrations. CTL3 with the YSU PBL scheme simulates stronger diurnal variation of surface PM_{2.5} concentrations than does CTL2 with the MYNN PBL scheme, primarily due to its larger diurnal variation of PBL

mixing. With less contribution from emissions to the surface PM_{2.5} concentrations, CTL2 and CTL3 simulate less primary PM_{2.5} (OIN, OM, BC) than does CTL1 (Fig. 5), particularly during the night when the PBL mixing is weak. This leads to the weaker diurnal variation of total surface PM_{2.5} concentrations in CTL2 and CTL3 as discussed above. The higher DI during the night in CTL3 than CTL2 can also be explained by the higher primary PM_{2.5} during the night due to weaker PBL mixing.

3.2.2 Sensitivity to the PBL mixing coefficient

The results discussed above suggest that the WRF-Chem-simulated diurnal variation of surface PM_{2.5} concentrations over East China is largely controlled by the PBL mixing process and is sensitive to the PBL scheme and vertical-layer configuration within the PBL. However, the increase in the number of vertical layers within the PBL and the use of different PBL schemes cannot reduce the modeling biases in diurnal variation of surface PM_{2.5} concentrations. Many previous studies investigated the PBL mixing of pollutants by establishing the relationship between surface pollutant concentration and PBL height. However, it is noteworthy that in most atmospheric models, the mixing of pollutants within the PBL is treated either as full mixing within the PBL heights (i.e., uniformly distributed within the PBL heights) or as calculated based on the mixing coefficient diagnosed from the PBL scheme. The former method represents the strongest PBL mixing and the surface concentrations can be largely influenced by the PBL heights. The latter one means that the pollutant mixing does not depend explicitly on PBL heights, although the PBL heights still reflect the boundary mixing strength.

In WRF-Chem, the PBL mixing of pollutants is treated with the second approach. In order to further examine the simulated PBL mixing process in this study, Fig. 6 shows the diurnal variation of PBL heights and PBL mixing coefficients below PBL heights in Hefei in January, April, July, and October of 2018 from WRF-Chem experiments CTL1, CTL2, and CTL3. The black line represents the PBL heights, while the contour shading represents the PBL mixing coefficients within the PBL heights. First of all, the PBL heights simulated from the three experiments all show evident diurnal variation, with the maximum in the daytime and the minimum during the night. The simulated PBL heights from CTL1 and CTL2 with the same PBL scheme (MYNN) show very similar diurnal patterns, indicating that the vertical layer configuration has a small impact on modeling PBL heights. Both experiments simulate the largest diurnal variation of PBL heights in summer, with a changing factor of ~ 10 from ~ 2 km in the afternoon to ~ 200 m in the early morning, and the smallest diurnal variation of PBL heights in winter, with a changing factor of 2 from ~ 700 m in the afternoon to ~ 350 m in the early morning. The CTL3 simulation with the YSU PBL scheme shows similar diurnal variations of PBL

heights to those from the CTL1 and CTL2 simulations. CTL3 simulates similar PBL heights during the daytime but lower values during the night, particularly in October. The simulated PBL heights are evaluated with the long-term averaged PBL heights, primarily for 08:00 and 20:00 LT (local time), derived from the air sounding observations available at the four stations of East China as reported in Guo et al. (2016) (Fig. S11). In general, throughout the four seasons, CTL3 with the YSU scheme simulates reasonable PBL heights in the early morning and night, while CTL1 and CTL2 with the MYNN scheme overestimate the PBL heights compared to the derived values. The comparison between simulations and observations (Figs. 2 and 3) suggests the positive modeling biases of DI during the night may be partly due to the underestimation of the PBL mixing during the night, which cannot be explained by the positive modeling biases of PBL heights during the night.

It should be noted that the PBL mixing coefficients within the PBL in all three experiments also exhibit evident diurnal variation with changing factors of ~ 1000 and ~ 50 in summer and winter, respectively, which are much larger than that of the PBL height in all seasons. More WRF experiments with different PBL schemes are conducted, and all show similar results, i.e., that the diurnal variation of PBL mixing coefficients is much stronger than that of PBL heights (not shown). With relatively large values of PBL mixing coefficients during the daytime, the emitted pollutants can be mixed up, roughly reaching the layer of PBL heights. Therefore, the PBL height is very critical for determining the surface pollutant mixing strength during the daytime. However, a weak PBL mixing coefficient during the night results in the emitted PM_{2.5} and its precursors staying near the surface (i.e., within the first layer of model) during the night not being mixed up in reaching the PBL height (Fig. S12). This leads to the large difference of DI between CTL1 and CTL2 with different thicknesses of the first model layer during the night, although they simulate similar PBL heights. As another example in autumn, the PBL heights during the night are lower in CTL3 than in CTL1, while the DI during the night is higher in CTL1 than in CTL3 (Fig. 3) due to the weak PBL mixing coefficients during the night that cannot mix the pollutants up to the PBL height. This further demonstrates that the WRF-Chem-simulated diurnal variation of surface PM_{2.5} concentration is not explicitly controlled by the PBL height, but instead by the PBL mixing coefficient. In fact, in WRF-Chem, there is an existing empirical parameterization to enhance the PBL mixing of pollutants in urban areas based on the strength of anthropogenic emissions. However, it is only applied to gas pollutants if the MOSAIC aerosol scheme is selected, as in this study. It also tends to enhance the mixing up to half the number of the model vertical layers, which is beyond the PBL in most cases during the night. In this study, in order to examine the sensitivity of simulated DI to the PBL mixing coefficient, the sensitivity experiments, EXP1 and EXP2, are conducted corresponding to CTL1 and

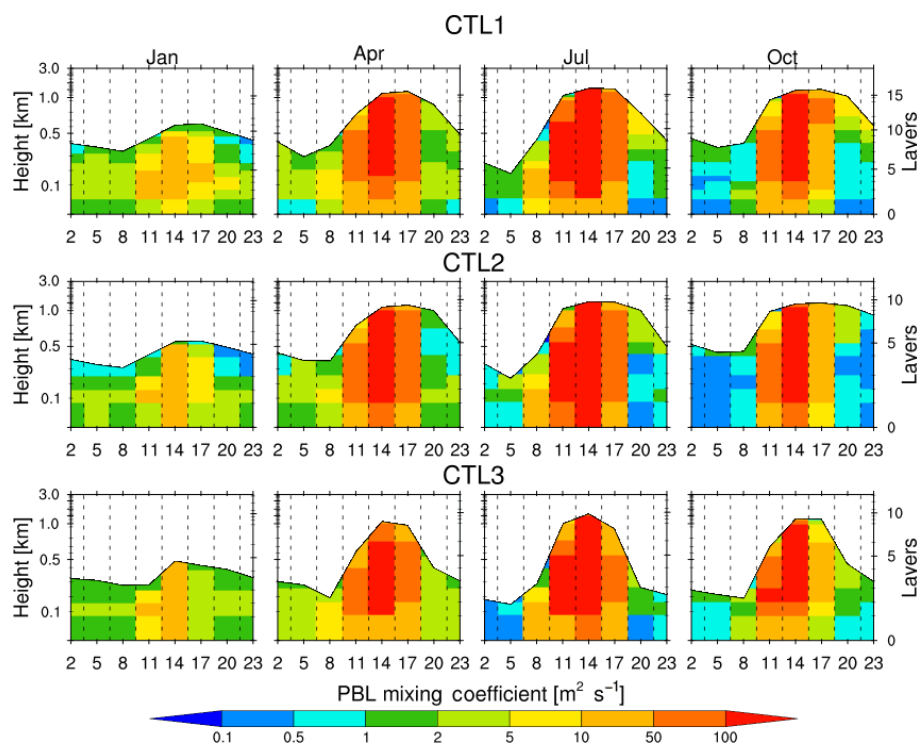


Figure 6. Diurnal variation of PBLH (planetary boundary layer height) and PBL mixing coefficient below PBLH averaged over Hefei for January, April, July, and October of 2018 from experiments CTL1, CTL2, and CTL3.

CTL2, respectively, by setting the lower limit of the PBL mixing coefficient from $0.1 \text{ m}^2 \text{ s}^{-1}$ (default in the publicly released version of WRF-Chem) to $5 \text{ m}^2 \text{ s}^{-1}$ within the PBL, which is applied to both gas and aerosol pollutants.

Figure 7 shows the simulated PBL height and mixing coefficients from the two sensitivity experiments, EXP1 and EXP2, in January, April, July, and October of 2018 in Hefei. It shows that the PBL mixing coefficient increases during the night within the PBL compared to the results shown in Fig. 6, while the values during the daytime remain almost the same. The difference of simulated surface PM_{2.5} between CTL1 and EXP1 is relatively small during the daytime, but significant during the night, which is because EXP1 can mix up the surface PM_{2.5} to the PBL heights during the night (Fig. S12). It is noteworthy that the lower limit parameter of $5 \text{ m}^2 \text{ s}^{-1}$ is entirely empirical. It is selected to represent the moderate mixing strength between the full PBL mixing and no PBL mixing. A few other values such as 1 and $10 \text{ m}^2 \text{ s}^{-1}$ are also tested. The results do not change the conclusions found in this study and therefore are not shown.

The change in PBL mixing coefficient during the night can significantly affect the diurnal variation of PBL mixing. Figure 8 shows the contribution of individual processes to the variation of surface PM_{2.5} concentrations every 3 h in Hefei simulated by EXP1 and EXP2 averaged for January, April, July, and October of 2018. The 3-hourly tendency of surface PM_{2.5} concentrations is also shown. As with Fig. 4, the con-

tributions and tendencies are divided by monthly mean surface PM_{2.5} concentrations for each month. The results for the other three cities (Nanjing, Hangzhou, Shanghai) are similar to that of Hefei and are shown in Fig. S13a–c. Compared to the results from CTL1 and CTL2 shown in Fig. 4, it is evident that the diurnal variation of tendency of surface PM_{2.5} concentrations is significantly reduced in all seasons. This mainly resulted from the significantly increased diurnal variation of the PBL mixing contribution. Specifically, the PBL mixing contribution during the night is increased. Figure 9 shows the diurnal variation of the surface concentration of each PM_{2.5} composition in Hefei simulated by EXP1 and EXP2 averaged for January, April, July, and October of 2018. The diurnal variations of surface concentrations of OM, BC, and OIN are significantly reduced primarily due to their reduced concentrations during the night in EXP1 and EXP2, compared to CTL1 and CTL2 (Fig. 5). The results for the other three cities (Nanjing, Hangzhou, Shanghai) are similar to that of Hefei and are shown in Fig. S14a–c.

The change in the PBL mixing and diurnal variation of primary PM_{2.5} near the surface turn out different DI. Figure 10 shows the diurnal variation of DI of surface PM_{2.5} averaged over the YRD region of East China for January, April, July, and October of 2018 from the observations and experiments CTL1, CTL2, EXP1, and EXP2. In general, the simulated DI is reduced significantly during the night in EXP1 and EXP2, much more consistent with the observations compared to

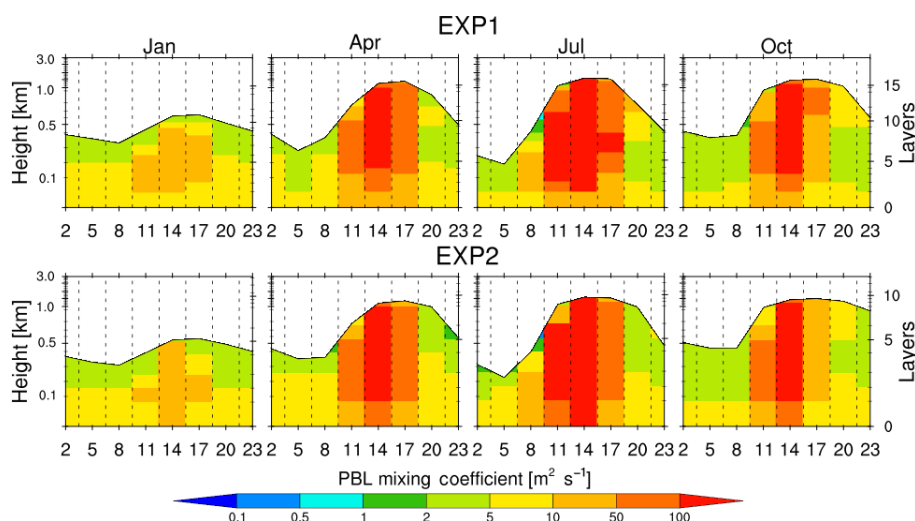


Figure 7. Diurnal variation of PBLH and PBL mixing coefficient below PBLH averaged over Hefei for January, April, July, and October of 2018 from experiments EXP1 and EXP2.

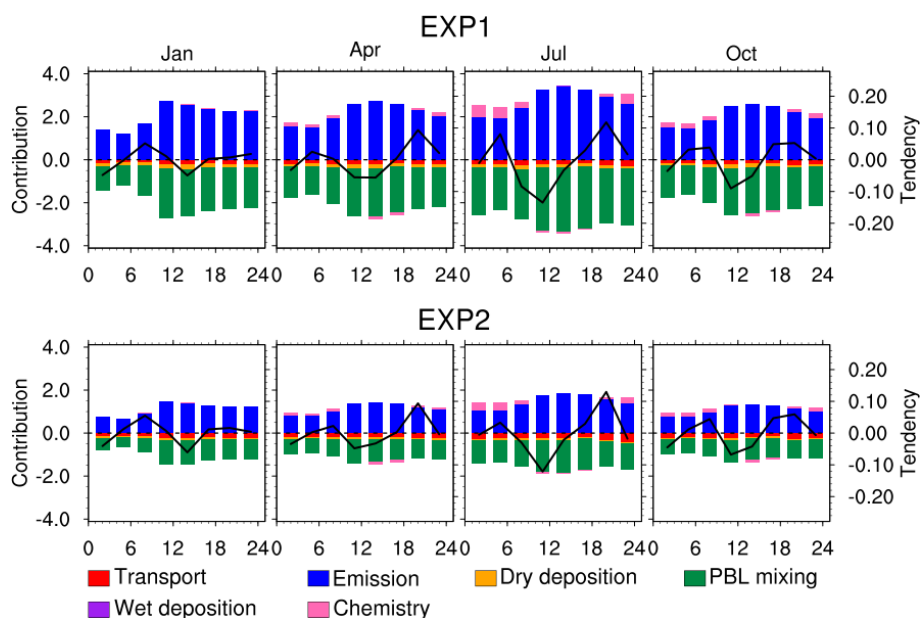


Figure 8. Relative contribution (normalized by monthly mean surface PM_{2.5} concentrations for each month) to surface PM_{2.5} concentrations every 3 h from individual process (transport, emission, dry and wet deposition, PBL mixing, chemical production/loss) averaged over Hefei for January, April, July, and October of 2018 from experiments EXP1 and EXP2. The 3-hourly relative tendency of surface PM_{2.5} concentrations is also shown as the black line.

the ones in CTL1 and CTL2. In spring, EXP1 and EXP2 slightly underestimate DI during night. Figure 11 shows the diurnal variation of DI averaged over the four cities for January, April, July, and October of 2018 from the observations and experiments CTL1, CTL2, EXP1, and EXP2. As discussed above, the diurnal variation of DI is much stronger in cities with relatively more emissions. The simulated DI is also more sensitive to the change in PBL mixing coefficient in these four cities compared to that on regional aver-

age. EXP1 and EXP2 produce much more consistent DI with the observations in the four cities than do CTL1 and CTL2 in all seasons. It is also noteworthy that the difference between EXP1 and EXP2 and that between CTL1 and CTL2 is reduced on both city average and regional average, which indicates that the enhanced PBL exchange coefficient during the night helps reduce the modeling sensitivity to the vertical layer configurations. The analysis above suggests that

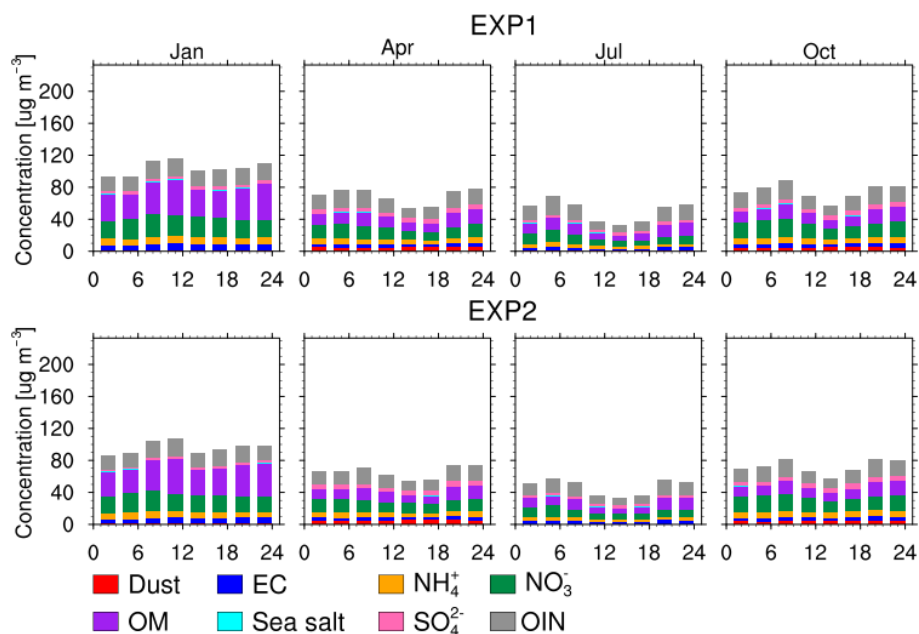


Figure 9. Diurnal cycle of surface PM_{2.5} composition concentrations (dust, OM, EC, sea salt, NH_4^+ , SO_4^{2-} , NO_3^- , and other inorganics) averaged over Hefei for January, April, July, and October of 2018 from experiments EXP1 and EXP2.

the simulated PBL mixing during the night in the publicly released WRF-Chem may be too weak.

Comparing the simulated surface concentrations of PM_{2.5} components between CTL1 (Fig. 5) and EXP1 (Fig. 9), it can be found that the daily average surface PM_{2.5} mass concentrations should also be reduced when the diurnal variation is reduced due to the reduction of nighttime surface PM_{2.5} concentrations. The model overestimates largely the monthly mean surface PM_{2.5} at the stations of East China in the seasons other than winter from the control experiments. These modeling biases are significantly reduced at most stations of East China (Fig. S15) in the sensitivity experiments. Figure 12 shows the comparison of monthly mean surface PM_{2.5} concentrations between the observations and the simulations from CTL1 and EXP1 at each observation site over the YRD region of East China for January, April, July, and October of 2018. In all seasons, CTL1 significantly overestimates the observed surface PM_{2.5} concentrations, with the normalized mean biases (NMBs) of 22 % (winter) to 109 % (summer) on regional average. EXP1 reduces the NMB to 7 % (winter) to 38 % (summer) on regional average. In CTL1, the NMB of the simulation exceeds 50 % at 20 %, 35 %, 65 %, and 60 % of observational sites over the YRD region of East China in January, April, July, and October, respectively, which reduces to 0 %, 10 %, 35 %, and 20 % of all sites in EXP1. In addition, EXP1 also increases the spatial correlation between observations and simulated results in all seasons (Fig. 12), although with the improvement of modeling diurnal variation EXP1 still cannot fully capture the observed spatial variability of surface PM_{2.5} concentrations among the observational

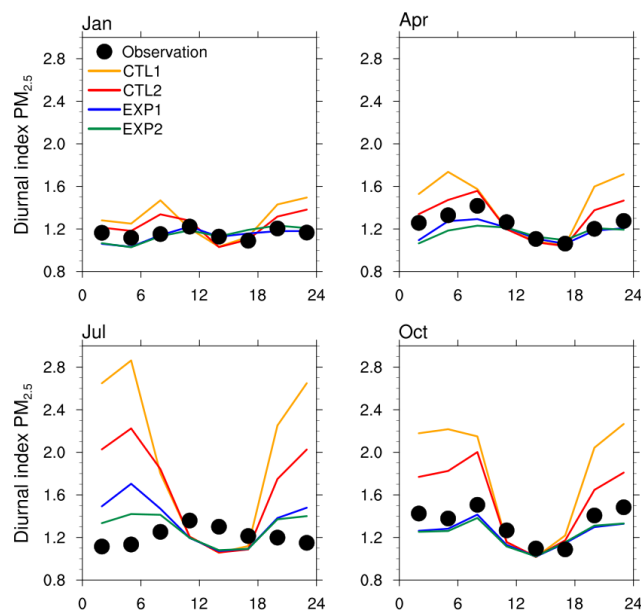


Figure 10. Diurnal index of surface PM_{2.5} concentrations within 24 h averaged over the YRD region of East China (within the black box of Fig. 1a) for January, April, July, and October of 2018 from experiments CTL1, CTL2, EXP1, and EXP2, and observations. Both the simulated results and observations are sampled at the model output frequency, i.e., 3-hourly.

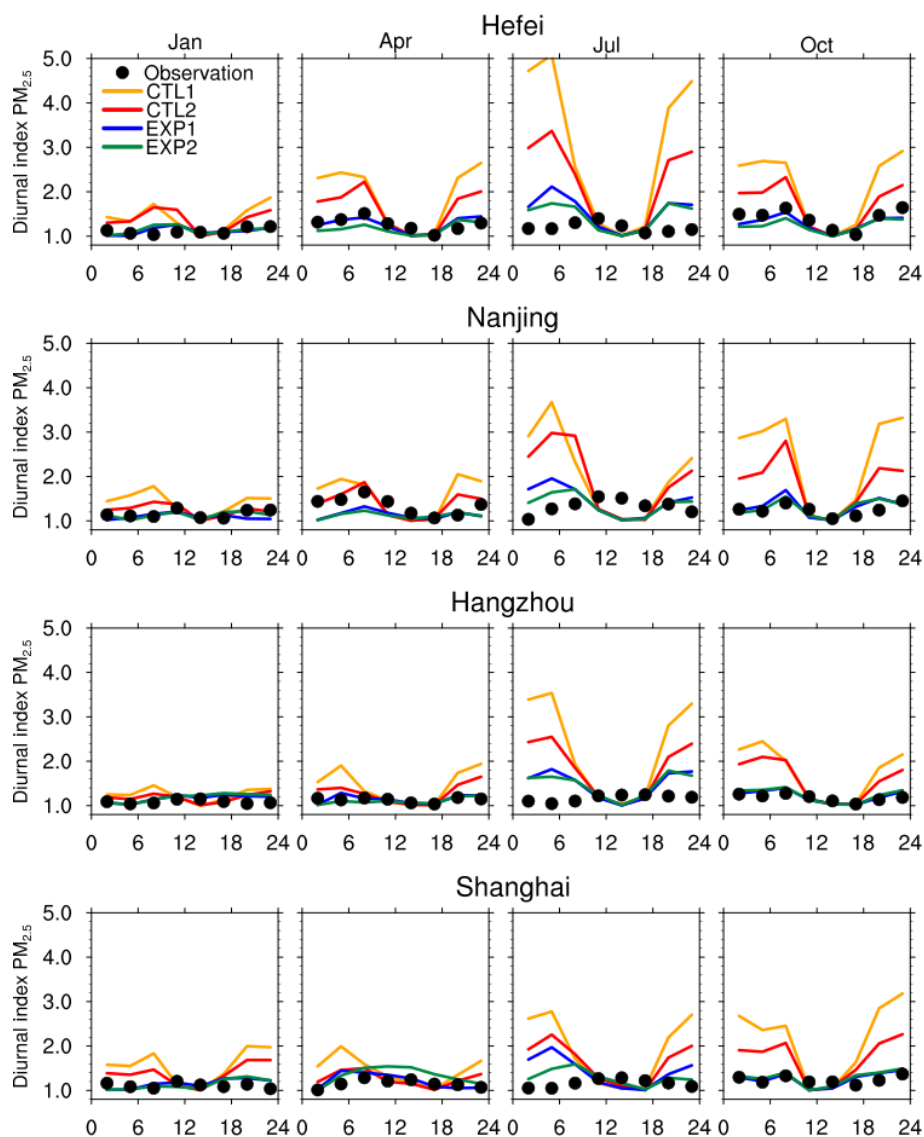


Figure 11. Diurnal index of surface PM_{2.5} concentrations within 24 h averaged over four cities (Hefei, Nanjing, Hangzhou, Shanghai) for January, April, July, and October of 2018 from experiments CTL1, CTL2, EXP1, and EXP2, and observations.

sites. This may be related to the biases in spatial distributions of emission and model processes contributed to the spatial variability of surface PM_{2.5} concentrations, which deserves further investigation in future.

3.3 Impacts from emission distributions

3.3.1 Impacts from emission diurnal variability

Besides the meteorology such as PBL mixing as discussed above, the diurnal variation of emissions may also play an important role in determining the DI of surface PM_{2.5} concentrations. One sensitivity experiment, EXP1_E1, without diurnal variation of anthropogenic emissions (Fig. 1c) is conducted. Figure 13 shows the spatial distribution of the differ-

ence in maximum DI between EXP1 and EXP1_E1 over East China. As removing diurnal variation of emissions will lead to more emissions during the night and thus increase the DI during the night over polluted areas, this generally results in a larger maximum DI. Therefore, EXP1 has a lower maximum DI than EXP1_E1 over most regions of East China in seasons other than winter. EXP1 could have a slightly larger maximum DI in winter when the diurnal variation of DI is relatively small (Figs. 2 and 3) and over the relatively clean region (Fig. 1a) in summer. Figure 14 shows the diurnal index of surface PM_{2.5} concentrations within 24 h averaged over the four cities for January, April, July, and October of 2018 from observations and the EXP1 and EXP1_E1 experiments. In general, EXP1 shows lower DI than EXP1_E1 during the night and therefore has a smaller diurnal variation

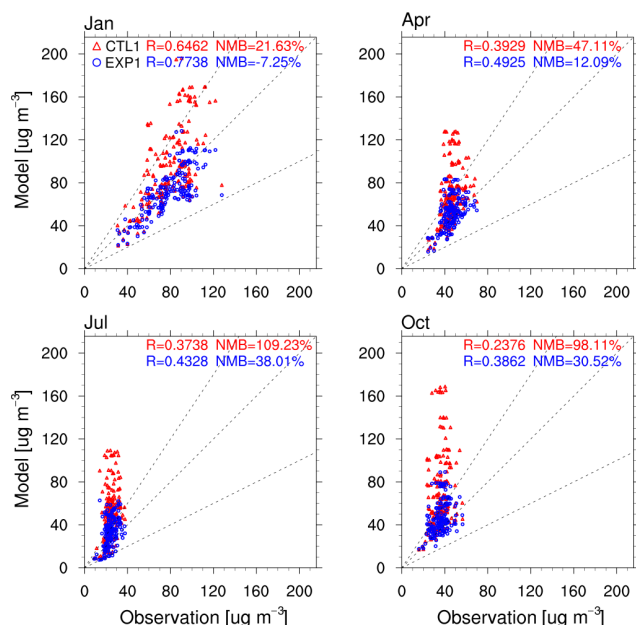


Figure 12. Comparison of monthly mean surface PM_{2.5} concentrations between the observations and the simulations from experiments CTL1 and EXP1 at each observation site over the YRD region of East China (as shown in Fig. 1a within the black box) for January, April, July, and October of 2018. The dashed lines represent -50 %, 0 %, and 50 % of the NMB of simulation.

of DI in four cities. The largest difference between EXP1 and EXP1_E1 in four cities exists in summer, and the smallest is in winter. Compared to the impacts from PBL mixing as shown in Fig. 11, the reduction of the diurnal variation of DI by adding the diurnal variation of anthropogenic emissions is much smaller.

Figure 13 shows that EXP1 with diurnal variation of emissions could simulate slightly larger diurnal variation of DI over the relatively clean region than EXP1_E1 in winter and summer. The higher DI in EXP1 than EXP1_E1 is primarily in the afternoon and evening (Fig. S16). One grid over southern Anhui is selected for analysis of contributions from different processes in the model to the diurnal variation of surface PM_{2.5} concentrations from experiments EXP1 and EXP1_E1 (Fig. 15). Different from the process contributions over the relatively polluted region (Fig. 8), the contribution from direct local emission to the surface PM_{2.5} concentrations is relatively small over the clean region. Instead, the contributions from chemistry, dry deposition, PBL mixing, and transport dominate the diurnal variation of surface PM_{2.5} concentrations. The PBL mixing could increase the surface PM_{2.5} concentrations during the daytime because of mixing down of the pollutants transported from polluted regions above the surface. The diurnal change in surface PM_{2.5} concentrations between EXP1 and EXP1_E1 is very similar, with a slight difference that results in their slight difference in DI in the afternoon and night.

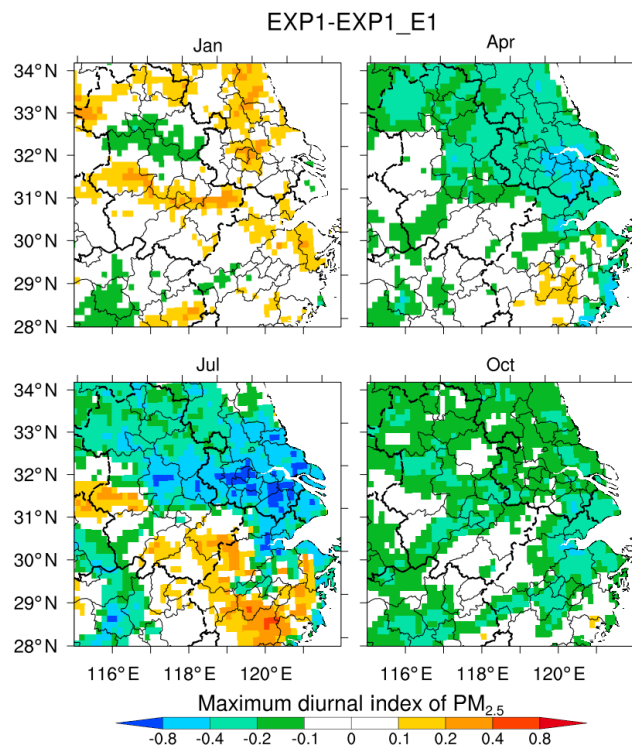


Figure 13. Spatial distribution of the difference in the daily maximum diurnal index of surface PM_{2.5} concentrations between experiments EXP1 and EXP1_E1 over East China in January, April, July, and October of 2018.

3.3.2 Impacts from emission injection height

Previous studies suggested that the injection height of emissions from power plants may also affect the diurnal cycle of surface pollutant concentrations, particularly for SO₂ (e.g., Wang et al., 2010; Lin et al., 2012; Qi et al., 2012; Xu et al., 2014). Therefore, one sensitivity experiment, EXP1_E2, is conducted by setting the anthropogenic emissions placed only in the first layer of the model. Figure 16 shows the spatial distribution of the difference in maximum DI between EXP1 and EXP1_E2 over East China. Over most areas of East China, EXP1 simulates lower maximum DI than EXP1_E2, and the difference is primarily in spring and summer. The impact of injection height is negligible in winter. The distribution of impacts correlates highly with the distribution of power plant locations. The reduction of the DI of surface SO₂ concentrations in EXP1 compared to EXP1_E2 is mainly due to more emissions being placed above the PBL during the night (Fig. S17). As shown in Table 2, most of the power plant emissions are placed below 500 m in EXP1. The larger impact in summer than in winter is mainly due to the higher PBL heights during the night in winter (Fig. 7). Therefore, emissions are still placed within the PBL even with the injection height, which results in the small difference of DI of surface SO₂ concentrations between EXP1 and EXP1_E2.

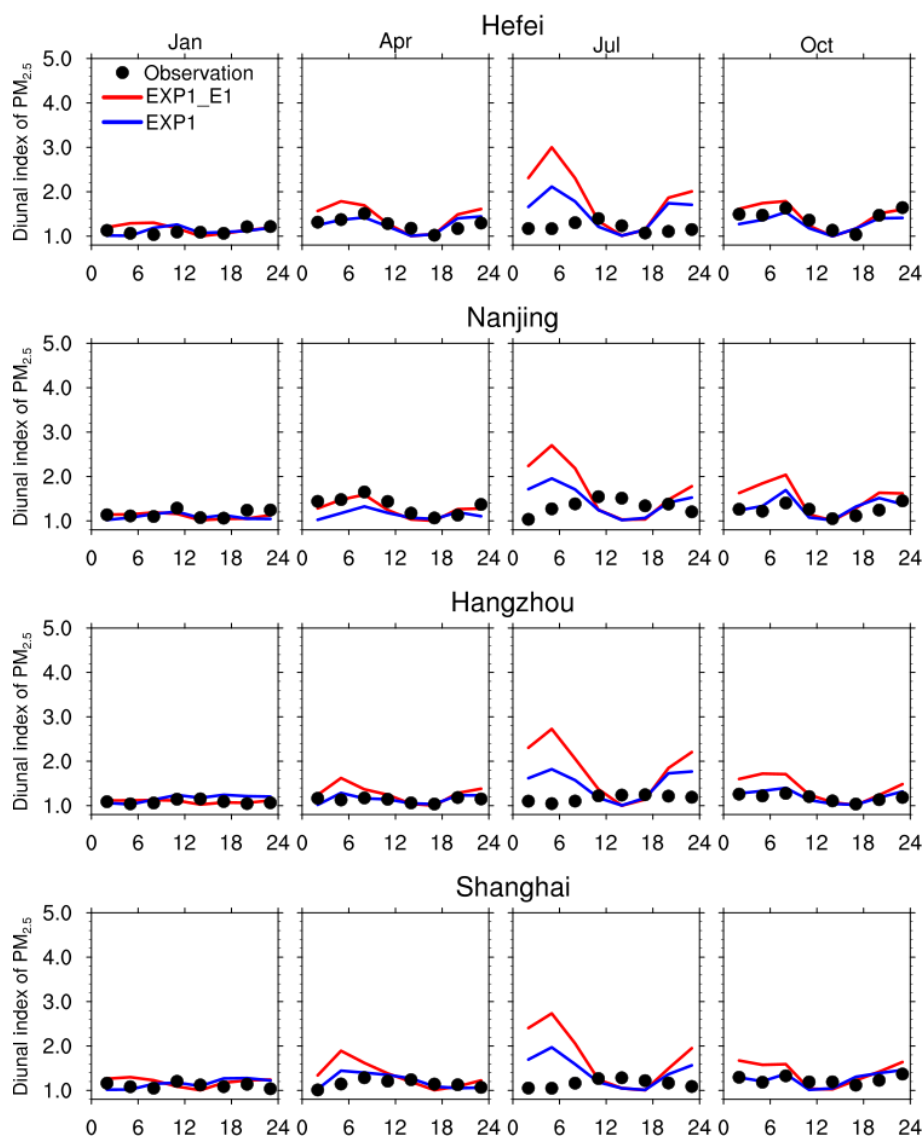


Figure 14. Diurnal index of surface PM_{2.5} concentrations within 24 h averaged over four cities (Hefei, Nanjing, Hangzhou, Shanghai) for January, April, July, and October of 2018 from experiments EXP1_E1 and EXP1 and observations.

For surface PM_{2.5} concentrations, the impact of emission injection height is even smaller and only distinguishable in summer (Fig. S18). Overall, the impact from the injection height of emissions on the diurnal variation of surface PM_{2.5} concentrations is much smaller than that from PBL mixing.

4 Summary

In this study, the observed characteristics of diurnal variation of surface PM_{2.5} concentrations over the YRD region of East China in four seasons of 2018 are examined based on the hourly surface observations at 190 stations of the region. On regional average, the observed diurnal variation is weakest in winter and strongest in autumn. In spring and autumn, the

observed patterns of diurnal variation are similar, showing the minimum surface PM_{2.5} concentration in the afternoon, consistent with previous studies (e.g., Zhang and Cao, 2015; Liu et al., 2016; Guo et al., 2017). In summer, different from other seasons, the observed diurnal variation shows the maximum surface PM_{2.5} concentration near noontime.

The WRF-Chem experiments generally capture the observed seasonality of diurnal variation of surface PM_{2.5} concentrations, except that in summer the model significantly overestimates the diurnal peak during the night and produces an opposite diurnal pattern with the minimum concentration near noontime. The model can generally reproduce the patterns with the minimum noontime concentration in spring and autumn, but overestimates the observed nighttime peaks, particularly in autumn. Emission and PBL mix-

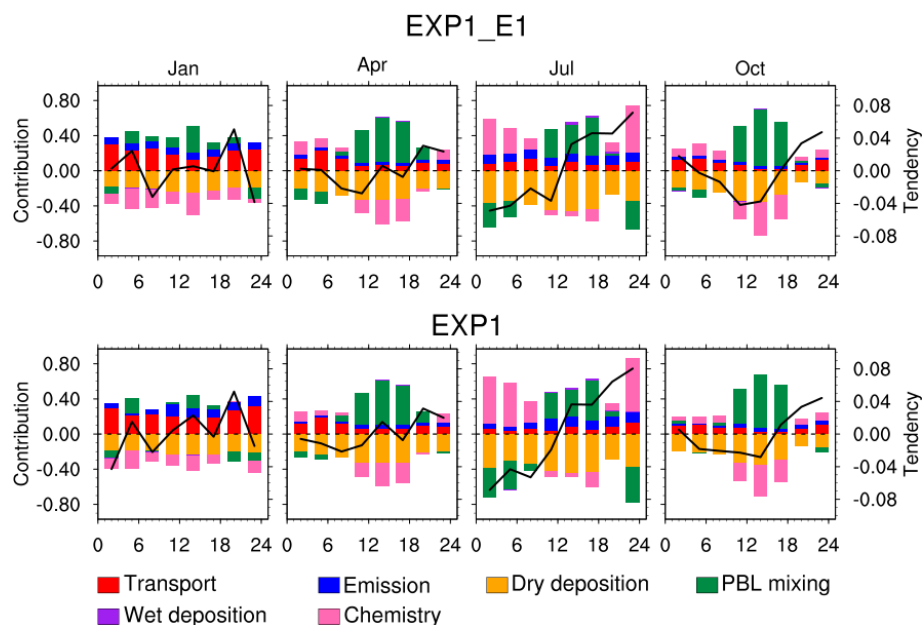


Figure 15. Relative contribution (normalized by monthly mean surface PM_{2.5} concentrations for each month) to surface PM_{2.5} concentrations every 3 h from individual processes (transport, emission, dry and wet deposition, PBL mixing, chemical production/loss) averaged over southern Anhui for January, April, July, and October of 2018 from experiments EXP1_E1 and EXP1. The 3-hourly relative tendency of surface PM_{2.5} concentrations is also shown as the black line.

ing are found to be the two dominant processes controlling the diurnal variation of surface PM_{2.5} concentrations over the polluted areas, and the PBL mixing leads to the simulated diurnal pattern of surface PM_{2.5} concentrations. More specifically, the simulations suggest that the PBL mixing of the primary PM_{2.5} determines the modeled diurnal variation of surface PM_{2.5} concentrations. Although the observation of PM_{2.5} components is not available to evaluate the diurnal variation of primary PM_{2.5}, the simulated diurnal variation of the surface mixing ratio of CO that is normally used to represent the primary pollutant is compared with the observations (Fig. S19). The results from experiments with enhanced nighttime PBL mixing are more consistent with the observations compared to the control experiments, which supports the findings about PM_{2.5}.

The modeling results are found to be sensitive to the PBL schemes and the vertical configuration (i.e., the number of model layers within the PBL) of simulations. However, none of the PBL schemes in WRF-Chem can reduce the modeling biases in diurnal variation of surface PM_{2.5} concentrations. Contrary to intuition, more model layers within the PBL worsen the model performance, which is mainly due to more layers within the PBL making the first model layer thinner and enlarging the contribution from emissions if PBL mixing is not efficient. The analysis indicates that although PBL height is an important factor in reflecting the PBL mixing strength, the PBL mixing process is more explicitly controlled by the PBL mixing coefficient instead of the height in WRF-Chem, particularly during the night. Increasing the

lower limit of the PBL mixing coefficient within the PBL can significantly reduce the modeling biases in diurnal variation of surface PM_{2.5} concentrations, primarily during the night. In addition, it can also reduce the modeling sensitivity to the model vertical configuration. The model performance of daily mean surface PM_{2.5} concentrations is also largely improved when the biases of diurnal variation are reduced. The diurnal variation of anthropogenic emissions and injection height of power plant emissions can affect the diurnal cycle of surface PM_{2.5} concentrations to some extent, but the impact is much smaller than that of PBL mixing.

5 Discussion

This study highlights the importance of modeling the PBL mixing coefficient within the PBL in models like WRF-Chem that simulate the PBL mixing process based on the mixing coefficient instead of PBL height. Some studies found that other models also overestimated the diurnal variation of observed surface PM_{2.5} concentrations over East China (e.g., Cai and Xie, 2011; M. Liu et al., 2018). Our finding suggests that those models may also have the problems in modeling PBL mixing during the night. Many previous modeling and observation studies focus on investigating the variation of PBL height and its interaction with aerosol concentration (e.g., Sawyer, 2015; Ding et al., 2013; Z. Li et al., 2017; Song et al., 2018; Su et al., 2018). However, this study reveals that the PBL mixing flux is also critical

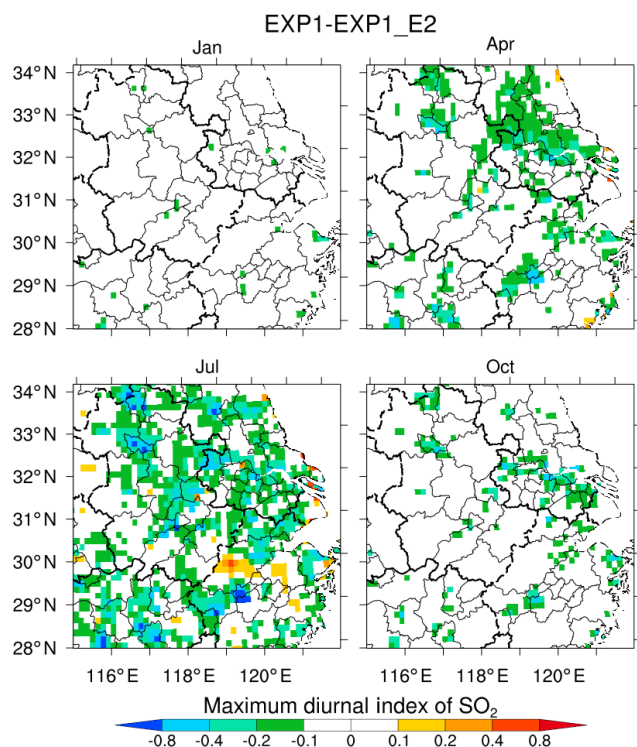


Figure 16. Spatial distribution of the difference in the daily maximum diurnal index of surface SO₂ concentrations between experiments EXP1_E2 and EXP1 over East China in January, April, July, and October of 2018.

in addition to the PBL height in terms of understanding the mixing of pollutants within the PBL, particularly during the night, which can significantly affect not only the diurnal variation, but also the daily mean of surface pollutant concentrations. The increase in PBL mixing during the night reduces the modeling biases, which may suggest that the simulated PBL mixing during the night in WRF-Chem is too weak. One possible reason may be the urban heat island effect that is not accounted for in this study, because the observation sites are mostly in urban or sub-urban areas. The test simulations with the current version of WRF-Chem using the Noah land surface model with an urban effect can increase the nighttime PBL mixing coefficient from 0.1 to 1–10 m² s^{−1} during some cases in urban areas, but the results are sensitive to the urban schemes (not shown), which deserves investigation in future. The model horizontal resolution may also affect the modeling results of PBL mixing and urbanization. However, one sensitivity experiment at 4 km horizontal resolution shows that the PBL mixing at the stations does not change significantly (not shown). The modeling at higher resolution particularly down to large-eddy scale deserves further investigation. Another suggestion is that the PBL mixing of pollutants may not be able to follow directly the mixing coefficient diagnosed by PBL parameterization for meteorology, which deserves further investigation. The improvement of modeling

PBL heights is not enough for understanding the PBL mixing of pollutants. In order to better understand PBL structure and the detailed mixing process, besides the observation or retrieval of PBL height, observations of PBL characteristics are needed.

Although the sensitivity adjustment of the PBL mixing coefficient during the night can largely reduce the modeling biases in diurnal variation of surface PM_{2.5} concentrations, one evident deficiency is that the model produces an opposite diurnal pattern compared with observations in summer. It needs to be noted that the WRF-Chem simulations conducted in this study do not consider the SOA production that still has large uncertainties in mechanisms. One sensitivity experiment with the SOA production shows that the model can better represent the observed diurnal pattern of surface PM_{2.5} concentrations in summer showing the maximum concentration in the daytime (Fig. S20). This indicates that the SOA production may be important for modeling the diurnal variation of surface PM_{2.5} concentrations in summer over East China, which suggests more detailed analysis of the impact of SOA production on the diurnal cycle of surface PM_{2.5} concentrations is needed with observations. It is also noteworthy that the impact of SOA production on diurnal variation of surface PM_{2.5} concentrations is only significant in summer, likely due to the strong photochemistry activity in summer. Another uncertainty of the results in this study may be related to emissions. Although the diurnal variation and injection height of emission do not contribute significantly to the nighttime positive biases of surface PM_{2.5} concentrations, the emission uncertainties of primary PM may influence the diurnal cycle of surface PM_{2.5}. For example, overestimation of primary PM emission can increase the diurnal variation. Therefore, this study suggests that the long-term measurements of PM_{2.5} components at more stations and the in situ measurements of vertical profiles of PM_{2.5} concentrations within the PBL during the night are needed to further investigate the characteristics of diurnal variation of PM_{2.5}, which can improve our understanding of the impacts of multiple processes, such as chemical production, emissions, and meteorology, on the formation and evolution of air pollution.

Data availability. The release version of WRF-Chem can be downloaded from http://www2.mmm.ucar.edu/wrf/users/download/get_source.html (last access: 5 March 2020) (WRF, 2020). The updated USTC version of WRF-Chem is available by downloading from <http://aemol.ustc.edu.cn/product/list/> (last access: 5 March 2020) (University of Science and Technology of China, 2020) or by contacting chunzhao@ustc.edu.cn. Also, the code modifications will be incorporated into the release version of WRF-Chem in future.

Supplement. The supplement related to this article is available online at: <https://doi.org/10.5194/acp-20-2839-2020-supplement>.

Author contributions. QD and CZ designed the experiments and conducted and analyzed the simulations. All the authors contributed to the discussion and final version of the paper.

Competing interests. The authors declare that they have no conflict of interest.

Acknowledgements. This research was supported by the Fundamental Research Funds for the Central Universities and the National Natural Science Foundation of China (grant 41775146). The study used the computing resources from the High-Performance Computing Center of the University of Science and Technology of China (USTC). Part of the observation data is from the Qingyue Open Environmental Data Center (<https://data.epmap.org>, last access: 5 March 2020).

Financial support. This research has been supported by the the National Natural Science Foundation of China (grant no. 41775146).

Review statement. This paper was edited by Yun Qian and reviewed by three anonymous referees.

References

- Ackerman, T. P.: A Model of the Effect of Aerosols on Urban Climates with Particular Applications to the Los Angeles Basin, *J. Atmos. Sci.*, 34, 531–547, [https://doi.org/10.1175/1520-0469\(1977\)034<0531:AMOTEO>2.0.CO;2](https://doi.org/10.1175/1520-0469(1977)034<0531:AMOTEO>2.0.CO;2), 1977.
- Arola, A., Eck, T. F., Huttunen, J., Lehtinen, K. E. J., Lindfors, A. V., Myhre, G., Smirnov, A., Tripathi, S. N., and Yu, H.: Influence of observed diurnal cycles of aerosol optical depth on aerosol direct radiative effect, *Atmos. Chem. Phys.*, 13, 7895–7901, <https://doi.org/10.5194/acp-13-7895-2013>, 2013.
- Barnard, J. C., Fast, J. D., Paredes-Miranda, G., Arnott, W. P., and Laskin, A.: Technical Note: Evaluation of the WRF-Chem “Aerosol Chemical to Aerosol Optical Properties” Module using data from the MILAGRO campaign, *Atmos. Chem. Phys.*, 10, 7325–7340, <https://doi.org/10.5194/acp-10-7325-2010>, 2010.
- Bei, N., Li, G., Huang, R.-J., Cao, J., Meng, N., Feng, T., Liu, S., Zhang, T., Zhang, Q., and Molina, L. T.: Typical synoptic situations and their impacts on the wintertime air pollution in the Guanzhong basin, China, *Atmos. Chem. Phys.*, 16, 7373–7387, <https://doi.org/10.5194/acp-16-7373-2016>, 2016.
- Binkowski, F. S. and Shankar, U.: The Regional Particulate Matter Model: 1. Model Description and Preliminary Results, *J. Geophys. Res.*, 100, 26191–26209, 1995.
- Cai, H. and Xie, S.: Traffic-related air pollution modeling during the 2008 Beijing Olympic Games: the effects of an odd-even day traffic restriction scheme, *Sci. Total Environ.*, 409, 1935–1948, <https://doi.org/10.1016/j.scitotenv.2011.01.025>, 2011.
- Chapman, E. G., Gustafson Jr., W. I., Easter, R. C., Barnard, J. C., Ghan, S. J., Pekour, M. S., and Fast, J. D.: Coupling aerosol-cloud-radiative processes in the WRF-Chem model: Investigating the radiative impact of elevated point sources, *Atmos. Chem. Phys.*, 9, 945–964, <https://doi.org/10.5194/acp-9-945-2009>, 2009.
- Chen, D., Cui, H., Zhao, Y., Yin, L., Lu, Y., and Wang, Q.: A two-year study of carbonaceous aerosols in ambient PM_{2.5} at a regional background site for western Yangtze River Delta, China, *Atmos. Res.*, 183, 351–361, <https://doi.org/10.1016/j.atmosres.2016.09.004>, 2017.
- Chen, S., Zhao, C., Qian, Y., Leung, L. R., Huang, J., Huang, Z., Bi, J., Zhang, W., Shi, J., Yang, L., Li, D., and Li, J.: Regional modeling of dust mass balance and radiative forcing over East Asia using WRF-Chem, *Aeolian Res.*, 15, 15–30, <https://doi.org/10.1016/j.aeolia.2014.02.001>, 2014.
- Chen, T., He, J., Lu, X., She, J., and Guan, Z.: Spatial and Temporal Variations of PM_{2.5} and Its Relation to Meteorological Factors in the Urban Area of Nanjing, China, *Int. J. Environ. Res. Publ. Health*, 13, 921, <https://doi.org/10.3390/ijerph13090921>, 2016.
- Chen, W., Tang, H., and Zhao, H.: Diurnal, weekly and monthly spatial variations of air pollutants and air quality of Beijing, *Atmos. Environ.*, 119, 21–34, <https://doi.org/10.1016/j.atmosenv.2015.08.040>, 2015.
- Cheng, Y., Zheng, G., Wei, C., Mu, Q., Zheng, B., Wang, Z., Gao, M., Zhang, Q., He, K., Carmichael, G., Pöschl, U., and Su, H.: Reactive nitrogen chemistry in aerosol water as a source of sulfate during haze events in China, *Sci. Adv.*, 2, e1601530, <https://doi.org/10.1126/sciadv.1601530>, 2016.
- Davidson, C. I., Phalen, R. F., and Solomon, P. A.: Airborne particulate matter and human health: A review, *Aerosol Sci. Tech.*, 39, 737–749, 2005.
- Dentener, F., Kinne, S., Bond, T., Boucher, O., Cofala, J., Geroso, S., Ginoux, P., Gong, S., Hoelzemann, J. J., Ito, A., Marelli, L., Penner, J. E., Putaud, J.-P., Textor, C., Schulz, M., van der Werf, G. R., and Wilson, J.: Emissions of primary aerosol and precursor gases in the years 2000 and 1750 prescribed data-sets for AeroCom, *Atmos. Chem. Phys.*, 6, 4321–4344, <https://doi.org/10.5194/acp-6-4321-2006>, 2006.
- Dickerson, R. R., Kondragunta, S., Stenchikov, G., Civerolo, K. L., Doddridge, B. G., and Holben, B. N.: The impact of aerosols on solar ultraviolet radiation and photochemical smog, *Science*, 278, 827–830, <https://doi.org/10.1126/science.278.5339.827>, 1997.
- Ding, A. J., Fu, C. B., Yang, X. Q., Sun, J. N., Petäjä, T., Kerminen, V.-M., Wang, T., Xie, Y., Herrmann, E., Zheng, L. F., Nie, W., Liu, Q., Wei, X. L., and Kulmala, M.: Intense atmospheric pollution modifies weather: a case of mixed biomass burning with fossil fuel combustion pollution in eastern China, *Atmos. Chem. Phys.*, 13, 10545–10554, <https://doi.org/10.5194/acp-13-10545-2013>, 2013.
- Easter, R. C., Ghan, S. J., Zhang, Y., Saylor, R. D., Chapman, E. G., Laulainen, N. S., Abdul-Razzak, H., Leung, L. R., Bian, X., and Zaveri, R. A.: MIRAGE: Model Description and Evaluation of Aerosols and Trace Gases, *J. Geophys. Res.*, 109, D20210, <https://doi.org/10.1029/2004JD004571>, 2004.
- Fast, J. D., Gustafson Jr., W. I., Easter, R. C., Zaveri, R. A., Barnard, J. C., Chapman, E. G., and Grell, G. A.: Evolution of ozone, particulates, and aerosol direct forcing in an urban area using a new fully-coupled meteorology, chemistry, and aerosol model, *J. Geophys. Res.*, 111, D21305, <https://doi.org/10.1029/2005JD006721>, 2006.

- Feng, J., Zhong, M., Xu, B., Du, Y., Wu, M., Wang, H., and Chen, C.: Concentrations, seasonal and diurnal variations of black carbon in PM_{2.5} in Shanghai, China, *Atmos. Res.*, 147–148, 1–9, <https://doi.org/10.1016/j.atmosres.2014.04.018>, 2014.
- Fu, Q., Zhuang, G., Wang, J., Xu, C., Huang, K., Li, J., Hou, B., Lu, T., and Streets, D. G.: Mechanism of formation of the heaviest pollution episode ever recorded in the Yangtze River Delta, China, *Atmos. Environ.*, 42, 2023–2036, <https://doi.org/10.1016/j.atmosenv.2007.12.002>, 2008.
- Gao, Y., Zhao, C., Liu, X., Zhang, M., and Leung, L. R.: WRF-Chem simulations of aerosols and anthropogenic aerosol radiative forcing in East Asia, *Atmos. Environ.*, 92, 250–266, <https://doi.org/10.1016/j.atmosenv.2014.04.038>, 2014.
- GBD Risk Factors Collaborators: Global, regional, and national comparative risk assessment of 84 behavioural, environmental and occupational, and metabolic risks or clusters of risks, 1990–2016: a systematic analysis for the Global Burden of Disease Study 2016, *Lancet*, 390, 1345–1422, 2017.
- Geng, G., Zhang, Q., Martin, R. V., van Donkelaar, A., Huo, H., Che, H., Lin, J., and He, K.: Estimating long-term PM_{2.5} concentrations in China using satellite-based aerosol optical depth and a chemical transport model, *Remote Sens. Environ.*, 166, 262–270, <https://doi.org/10.1016/j.rse.2015.05.016>, 2015.
- Ginoux, P., Chin, M., Tegen, I., Prospero, J. M., Holben, B., Dubovik, O., and Lin, S.: Sources and distributions of dust aerosols simulated with the GOCART model, *J. Geophys. Res.*, 106, 20225–20273, 2001.
- Gong, D.-Y., Ho, C.-H., Chen, D., Qian, Y., Choi, Y.-S., and Kim, J.: Weekly cycle of aerosol-meteorology interaction over China, *J. Geophys. Res.*, 112, L03819, <https://doi.org/10.1029/2007JD008888>, 2007.
- Gong, S. L.: A parameterization of sea-salt aerosol source function for sub- and super-micron particles, *Global Biogeochem. Cy.*, 17, 1097, <https://doi.org/10.1029/2003GB002079>, 2003.
- Grell, G. A., Peckham, S. E., Schmitz, R., and McKeen, S. A., Frost, G., Skamarock, W. C., and Eder, B.: Fully coupled “online” chemistry within the WRF model, *Atmos. Environ.*, 39, 6957–6976, 2005.
- Gu, Z., Feng, J., Han, W., Li, L., Wu, M., Fu, J., and Sheng, G.: Diurnal variations of polycyclic aromatic hydrocarbons associated with PM_{2.5} in Shanghai, China, *J. Environ. Sci.*, 22, 389–396, 2010.
- Guo, J., Miao, Y., Zhang, Y., Liu, H., Li, Z., Zhang, W., He, J., Lou, M., Yan, Y., Bian, L., and Zhai, P.: The climatology of planetary boundary layer height in China derived from radiosonde and reanalysis data, *Atmos. Chem. Phys.*, 16, 13309–13319, <https://doi.org/10.5194/acp-16-13309-2016>, 2016.
- Guo, H., Cheng, T., Gu, X., Wang, Y., Chen, H., Bao, F., Shi, S., Xu, B., Wang, W., Zuo, X., Zhang, X., and Meng, C.: Assessment of PM_{2.5} concentrations and exposure throughout China using ground observations, *The Sci. Total Environ.*, 601–602, 1024–1030, <https://doi.org/10.1016/j.scitotenv.2017.05.263>, 2017.
- Guo, J., Xia, F., Zhang, Y., Liu, H., Li, J., Lou, M., He, J., Yan, Y., Wang, F., Min, M., and Zhai, P.: Impact of diurnal variability and meteorological factors on the PM_{2.5}–AOD relationship: Implications for PM_{2.5} remote sensing, *Environ. Poll.*, 221, 94–104, <https://doi.org/10.1016/j.envpol.2016.11.043>, 2017.
- Gustafson, W. I., Chapman, E. G., Ghan, S. J., Easter, R. C., and Fast, J. D.: Impact on modeled cloud characteristics due to simplified treatment of uniform cloud condensation nuclei during NEAQS 2004, *Geophys. Res. Lett.*, 34, L19809, <https://doi.org/10.1029/2007GL030021>, 2007.
- Ho, H. C., Wong, M. S., Yang, L., Shi, W., Yang, J., Bilal, M., and Chan, T.-C.: Spatiotemporal influence of temperature, air quality, and urban environment on cause-specific mortality during hazy days, *Environ. Int.*, 112, 10–22, <https://doi.org/10.1016/j.envint.2017.12.001>, 2018.
- Hong, S.-Y., Noh, Y., and Dudhia, J.: A New Vertical Diffusion Package with an Explicit Treatment of Entrainment Processes, *Mon. Weather Rev.*, 134, 2318–2341, <https://doi.org/10.1175/MWR3199.1>, 2006.
- Hu, J., Wang, Y., Ying, Q., and Zhang, H.: Spatial and temporal variability of PM_{2.5} and PM₁₀ over the North China Plain and the Yangtze River Delta, China, *Atmos. Environ.*, 95, 598–609, <https://doi.org/10.1016/j.atmosenv.2014.07.019>, 2014.
- Hu, J., Chen, J., Ying, Q., and Zhang, H.: One-year simulation of ozone and particulate matter in China using WRF/CMAQ modeling system, *Atmos. Chem. Phys.*, 16, 10333–10350, <https://doi.org/10.5194/acp-16-10333-2016>, 2016.
- Hu, Z., Huang, J., Zhao, C., Bi, J., Jin, Q., Qian, Y., Leung, L. R., Feng, T., Chen, S., and Ma, J.: Modeling the contributions of Northern Hemisphere dust sources to dust outflow from East Asia, *Atmos. Environ.*, 202, 234–243, <https://doi.org/10.1016/j.atmosenv.2019.01.022>, 2019.
- Hu, Z., Zhao, C., Huang, J., Leung, L. R., Qian, Y., Yu, H., Huang, L., and Kalashnikova, O. V.: Trans-Pacific transport and evolution of aerosols: evaluation of quasi-global WRF-Chem simulation with multiple observations, *Geosci. Model Dev.*, 9, 1725–1746, <https://doi.org/10.5194/gmd-9-1725-2016>, 2016.
- Huang, G., Cheng, T., Zhang, R., Tao, J., Leng, C., Zhang, Y., Zha, S., Zhang, D., Li, X., and Xu, C.: Optical properties and chemical composition of PM_{2.5} in Shanghai in the spring of 2012, *Particuology*, 13, 52–59, <https://doi.org/10.1016/j.partic.2013.10.005>, 2014.
- Huang, X., Ding, A., Liu, L., Liu, Q., Ding, K., Niu, X., Nie, W., Xu, Z., Chi, X., Wang, M., Sun, J., Guo, W., and Fu, C.: Effects of aerosol–radiation interaction on precipitation during biomass-burning season in East China, *Atmos. Chem. Phys.*, 16, 10063–10082, <https://doi.org/10.5194/acp-16-10063-2016>, 2016.
- Huang, X.-F., He, L.-Y., Hu, M., Canagaratna, M. R., Sun, Y., Zhang, Q., Zhu, T., Xue, L., Zeng, L.-W., Liu, X.-G., Zhang, Y.-H., Jayne, J. T., Ng, N. L., and Worsnop, D. R.: Highly time-resolved chemical characterization of atmospheric submicron particles during 2008 Beijing Olympic Games using an Aerodyne High-Resolution Aerosol Mass Spectrometer, *Atmos. Chem. Phys.*, 10, 8933–8945, <https://doi.org/10.5194/acp-10-8933-2010>, 2010.
- Iacono, M. J., Mlawer, E. J., Clough, S. A., and Morcrette, J. J.: Impact of an improved longwave radiation model, RRTM, on the energy budget and thermodynamic properties of the NCAR community climate model, CCM3, *J. Geophys. Res.-Atmos.*, 105, 14873–14890, 2000.
- Jacobson, M. Z.: Studying the effects of aerosols on vertical photolysis rate coefficient and temperature profiles over an urban airshed, *J. Geophys. Res.*, 103, 10593–10604, <https://doi.org/10.1029/98JD00287>, 1998.
- Jaeglé, L., Quinn, P. K., Bates, T. S., Alexander, B., and Lin, J.-T.: Global distribution of sea salt aerosols: new constraints from

- situ and remote sensing observations, *Atmos. Chem. Phys.*, 11, 3137–3157, <https://doi.org/10.5194/acp-11-3137-2011>, 2011.
- Janssens-Maenhout, G., Crippa, M., Guizzardi, D., Dentener, F., Muntean, M., Pouliot, G., Keating, T., Zhang, Q., Kurokawa, J., Wankmüller, R., Denier van der Gon, H., Kuenen, J. J. P., Klimont, Z., Frost, G., Darras, S., Koffi, B., and Li, M.: HTAP_v2.2: a mosaic of regional and global emission grid maps for 2008 and 2010 to study hemispheric transport of air pollution, *Atmos. Chem. Phys.*, 15, 11411–11432, <https://doi.org/10.5194/acp-15-11411-2015>, 2015.
- Jia, M., Zhao, T., Cheng, X., Gong, S., Zhang, X., Tang, L., Liu, D., Wu, X., Wang, L., and Chen, Y.: Inverse Relations of PM_{2.5} and O₃ in Air Compound Pollution between Cold and Hot Seasons over an Urban Area of East China, *Atmosphere*, 8, 59, <https://doi.org/10.3390/atmos8030059>, 2017.
- Jiang, F., Liu, Q., Huang, X., Wang, T., Zhuang, B., and Xie, M.: Regional modeling of secondary organic aerosol over China using WRF/Chem, *J. Aerosol Sci.*, 43, 57–73, <https://doi.org/10.1016/j.jaerosci.2011.09.003>, 2012.
- Kain, J. S.: The Kain–Fritsch convective parameterization: An update, *J. Appl. Meteorol.*, 43, 170–181, 2004.
- Kassianov, E., Barnard, J., Pekour, M., Berg, L. K., Michalsky, J., Lantz, K., and Hodges, G.: Do diurnal aerosol changes affect daily average radiative forcing?, *Geophys. Res. Lett.*, 40, 3265–3269, <https://doi.org/10.1002/grl.50567>, 2013.
- Kok, J. F.: A scaling theory for the size distribution of emitted dust aerosols suggests climate models underestimate the size of the global dust cycle, *P. Natl. Acad. Sci. USA*, 108, 1016–1021, <https://doi.org/10.1073/pnas.1014798108>, 2011.
- Kuang, Y., Zhao, C. S., Tao, J. C., and Ma, N.: Diurnal variations of aerosol optical properties in the North China Plain and their influences on the estimates of direct aerosol radiative effect, *Atmos. Chem. Phys.*, 15, 5761–5772, <https://doi.org/10.5194/acp-15-5761-2015>, 2015.
- Li, G., Wang, Y., Lee, K. H., Diao, Y., and Zhang, R.: Impacts of aerosols on the development and precipitation of a mesoscale squall line, *J. Geophys. Res.-Atmos.*, 114, D17205, <https://doi.org/10.1029/2008JD011581>, 2009.
- Li, J., Wang, G., Aggarwal, S. G., Huang, Y., Ren, Y., Zhou, B., Singh, K., Gupta, P. K., Cao, J., and Zhang, R.: Comparison of abundances, compositions and sources of elements, inorganic ions and organic compounds in atmospheric aerosols from Xi'an and New Delhi, two megacities in China and India, *Sci. Total Environ.*, 476–477, 485–495, <https://doi.org/10.1016/j.scitotenv.2014.01.011>, 2014.
- Li, J., Yang, W., Wang, Z., Chen, H., Hu, B., Li, J., Sun, Y., Fu, P., and Zhang, Y.: Modeling study of surface ozone source-receptor relationships in East Asia, *Atmos. Res.*, 167, 77–88, <https://doi.org/10.1016/j.atmosres.2015.07.010>, 2016.
- Li, M., Liu, H., Geng, G., Hong, C., Liu, F., Song, Y., Tong, D., Zheng, B., Cui, H., Man, H., Zhang, Q., and He, K.: Anthropogenic emission inventories in China: a review, *Nat. Sci. Rev.*, 4, 834–866, <https://doi.org/10.1093/nsr/nwx150>, 2017a.
- Li, M., Zhang, Q., Kurokawa, J.-I., Woo, J.-H., He, K., Lu, Z., Ohara, T., Song, Y., Streets, D. G., Carmichael, G. R., Cheng, Y., Hong, C., Huo, H., Jiang, X., Kang, S., Liu, F., Su, H., and Zheng, B.: MIX: a mosaic Asian anthropogenic emission inventory under the international collaboration framework of the MICS-Asia and HTAP, *Atmos. Chem. Phys.*, 17, 935–963, <https://doi.org/10.5194/acp-17-935-2017>, 2017b.
- Li, P., Wang, L., Guo, P., Yu, S., Mehmood, K., Wang, S., Liu, W., Seinfeld, J. H., Zhang, Y., Wong, D. C., Alapaty, K., Pleim, J., and Mathur, R.: High reduction of ozone and particulate matter during the 2016 G-20 summit in Hangzhou by forced emission controls of industry and traffic, *Environ. Chem. Lett.*, 15, 709–715, <https://doi.org/10.1007/s10311-017-0642-2>, 2017.
- Li, R., Li, Z., Gao, W., Ding, W., Xu, Q., and Song, X.: Diurnal, seasonal, and spatial variation of PM_{2.5} in Beijing, *Sci. Bull.*, 60, 387–395, 2015.
- Li, T., Horton, R. M., Bader, D. A., Liu, F., Sun, Q., and Kinney, P. L.: Long-term projections of temperature-related mortality risks for ischemic stroke, hemorrhagic stroke, and acute ischemic heart disease under changing climate in Beijing, China, *Environ. Int.*, 112, 1–9, <https://doi.org/10.1016/j.envint.2017.12.006>, 2018.
- Li, Z., Guo, J., Ding, A., Liao, H., Liu, J., Sun, Y., Wang, T., Xue, H., Zhang, H., and Zhu, B.: Aerosol and boundary-layer interactions and impact on air quality, *Nat. Sci. Rev.*, 4, 810–833, 2017.
- Liao, J., Wang, T., Wang, X., Xie, M., Jiang, Z., Huang, X., and Zhu, J.: Impacts of different urban canopy schemes in WRF/Chem on regional climate and air quality in Yangtze River Delta, China, *Atmos. Res.*, 145–146, 226–243, <https://doi.org/10.1016/j.atmosres.2014.04.005>, 2014.
- Lin, M., Tao, J., Chan, C.-Y., Cao, J.-J., Zhang, Z.-S., Zhu, L.-H., and Zhang, R.-J.: Regression Analyses between Recent Air Quality and Visibility Changes in Megacities at Four Haze Regions in China, *Aerosol Air Qual. Res.*, 12, 1049–1061, <https://doi.org/10.4209/aaqr.2011.11.0220>, 2012.
- Lin, W., Xu, X., Ma, Z., Zhao, H., Liu, X., and Wang, Y.: Characteristics and recent trends of sulfur dioxide at urban, rural, and background sites in north China: effectiveness of control measures, *J. Environ. Sci.*, 24, 34–49, 2012.
- Liu, J., Li, J., and Li, W.: Temporal Patterns in Fine Particulate Matter Time Series in Beijing: A Calendar View, *Scient. Rep.*, 6, 32221, <https://doi.org/10.1038/srep32221>, 2016.
- Liu, M., Lin, J., Wang, Y., Sun, Y., Zheng, B., Shao, J., Chen, L., Zheng, Y., Chen, J., Fu, T.-M., Yan, Y., Zhang, Q., and Wu, Z.: Spatiotemporal variability of NO₂ and PM_{2.5} over Eastern China: observational and model analyses with a novel statistical method, *Atmos. Chem. Phys.*, 18, 12933–12952, <https://doi.org/10.5194/acp-18-12933-2018>, 2018.
- Liu, S., Hua, S., Wang, K., Qiu, P., Liu, H., Wu, B., Shao, P., Liu, X., Wu, Y., Xue, Y., Hao, Y., and Tian, H.: Spatial-temporal variation characteristics of air pollution in Henan of China: Localized emission inventory, WRF/Chem simulations and potential source contribution analysis, *Sci. Total Environ.*, 624, 396–406, <https://doi.org/10.1016/j.scitotenv.2017.12.102>, 2018.
- Liu, T., Cai, Y., Feng, B., Cao, G., Lin, H., Xiao, J., Li, X., Liu, S., Pei, L., Fu, L., Yang, X., Zhang, B., and Ma, W.: Long-term mortality benefits of air quality improvement during the twelfth five-year-plan period in 31 provincial capital cities of China, *Atmos. Environ.*, 173, 53–61, <https://doi.org/10.1016/j.atmosenv.2017.10.054>, 2018.
- Liu, X.-Y., Zhang, Y., Zhang, Q., and He, K.-B.: Application of online-coupled WRF/Chem-MADRID in East Asia: Model evaluation and climatic effects of an-

- thropogenic aerosols, *Atmos. Environ.*, 124, 321–336, <https://doi.org/10.1016/j.atmosenv.2015.03.052>, 2016.
- Ma, Y., Xu, X., Song, W., Geng, F., and Wang, L.: Seasonal and diurnal variations of particulate organosulfates in urban Shanghai, China, *Atmos. Environ.*, 85, 152–160, <https://doi.org/10.1016/j.atmosenv.2013.12.017>, 2014.
- Mellor, G. L. and Yamada, T.: Development of a turbulence closure model for geophysical fluid problems, *Rev. Geophys.*, 20, 851–875, 1982.
- Menut, L., Goussebaile, A., Bessagnet, B., Khvorostyanov, D., and Ung, A.: Impact of realistic hourly emissions profiles on air pollutants concentrations modelled with CHIMERE, *Atmos. Environ.*, 49, 233–244, <https://doi.org/10.1016/j.atmosenv.2011.11.057>, 2012.
- Mlawer, E. J., Taubman, S. J., Brown, P. D., Iacono, M. J., and Clough, S. A.: Radiative transfer for inhomogeneous atmosphere: RRTM, a validated correlated-k model for the longwave, *J. Geophys. Res.*, 102, 16663–16682, 1997.
- Morrison, H., Thompson, G., and Tatarskii, V.: Impact of Cloud Microphysics on the Development of Trailing Stratiform Precipitation in a Simulated Squall Line: Comparison of One- and Two-Moment Schemes, *Mon. Weather Rev.*, 137, 991–1007, 2009.
- Nakanishi, M. and Niino, H.: An Improved Mellor–Yamada Level-3 Model: Its Numerical Stability and Application to a Regional Prediction of Advection Fog, *Bound.-Lay. Meteorol.*, 119, 397–407, <https://doi.org/10.1007/s10546-005-9030-8>, 2006.
- Ni, Z.-Z., Luo, K., Zhang, J.-X., Feng, R., Zheng, H.-X., Zhu, H.-R., Wang, J.-F., Fan, J.-R., Gao, X., and Cen, K.-F.: Assessment of winter air pollution episodes using long-range transport modeling in Hangzhou, China, during World Internet Conference, 2015, *Environ. Poll.*, 236, 550–561, <https://doi.org/10.1016/j.envpol.2018.01.069>, 2018.
- Noh, Y., Cheon, W.-G., Hong, S.-Y., and Raasch, S.: Improvement of the K-profile model for the planetary boundary layer based on large eddy simulation data, *Bound.-Lay. Meteorol.*, 107, 401–427, <https://doi.org/10.1023/A:1022146015946>, 2003.
- Pal, S., Lee, T. R., Phelps, S., and de Wekker, S. F. J.: Impact of atmospheric boundary layer depth variability and wind reversal on the diurnal variability of aerosol concentration at a valley site, *Sci. Total Environ.*, 496, 424–434, <https://doi.org/10.1016/j.scitotenv.2014.07.067>, 2014.
- Pathak, R. K., Wang, T., and Wu, W. S.: Nighttime enhancement of PM_{2.5} nitrate in ammonia-poor atmospheric conditions in Beijing and Shanghai: Plausible contributions of heterogeneous hydrolysis of N₂O₅ and HNO₃ partitioning, *Atmos. Environ.*, 45, 1183–1191, <https://doi.org/10.1016/j.atmosenv.2010.09.003>, 2011.
- Petäjä, T., Järvi, L., Kerminen, V.-M., Ding, A. J., Sun, J. N., Nie, W., Kujansuu, J., Virkkula, A., Yang, X.-Q., Fu, C. B., Zilitinkevich, S., and Kulmala, M.: Enhanced air pollution via aerosol-boundary layer feedback in China, *Scient. Rep.*, 6, 18998, <https://doi.org/10.1038/srep18998>, 2016.
- Pope III, C. A. and Dockery, D. W.: Health effects of fine particulate air pollution: lines that connect, *J. Air Waste Manage. Assoc.*, 56, 709–742, 2006.
- Powers, J. G., Klemp, J. B., Skamarock, W. C., Davis, C. A., Dudhia, J., Gill, D. O., Coen, J. L., Gochis, D. J., Ahmadov, R., Peckham, S. E., Grell, G. A., Michalakes, J., Trahan, S., Benjamin, S. G., Alexander, C. R., Dimego, G. J., Wang, W., Schwartz, C. S., Romine, G. S., Liu, Z., Snyder, C., Chen, F., Barlage, M. J., Yu, W., and Duda, M. G.: The Weather Research and Forecasting Model Overview System Efforts, and Future Directions, *B. Am. Meteorol. Soc.*, 98, 1717–1737, <https://doi.org/10.1175/bams-d-15-00308.1>, 2017.
- Qi, H., Lin, W., Xu, X., Yu, X., and Ma, Q.: Significant downward trend of SO₂ observed from 2005 to 2010 at a background station in the Yangtze Delta region, China, *Sci. China Chem.*, 55, 1451–1458, <https://doi.org/10.1007/s11426-012-4524-y>, 2012.
- Quan, J., Gao, Y., Zhang, Q., Tie, X., Cao, J., Han, S., Meng, J., Chen, P., and Zhao, D.: Evolution of planetary boundary layer under different weather conditions, and its impact on aerosol concentrations, *Particuology*, 11, 34–40, <https://doi.org/10.1016/j.partic.2012.04.005>, 2013.
- Roig Rodelas, R., Perdrix, E., Herbin, B., and Riffault, V.: Characterization and variability of inorganic aerosols and their gaseous precursors at a suburban site in northern France over one year (2015–2016), *Atmos. Environ.*, 200, 142–157, <https://doi.org/10.1016/j.atmosenv.2018.11.041>, 2019.
- Sawyer, V. R.: Interaction between aerosol and the planetary boundary layer depth at sites in the US and China, in: AGU Fall Meeting Abstracts, 14–18 December 2015, San Francisco, CA, 2015.
- Seaman, N. L., Stauffer, D. R., and Lario-Gibbs, A. M.: A Multiscale Four-Dimensional Data Assimilation System Applied in the San Joaquin Valley during SARMAP. Part I: Modeling Design and Basic Performance Characteristics, *J. Appl. Meteorol.*, 34, 1739–1761, [https://doi.org/10.1175/1520-0450\(1995\)034<1739:AMFDDA>2.0.CO;2](https://doi.org/10.1175/1520-0450(1995)034<1739:AMFDDA>2.0.CO;2), 1995.
- Seaton, A., MacNee, W., Donaldson, K., and Godden, D.: Particulate air pollution and acute health effects, *Lancet*, 345, 176–178, [https://doi.org/10.1016/s0140-6736\(95\)90173-6](https://doi.org/10.1016/s0140-6736(95)90173-6), 1995.
- Skamarock, W. C., Klemp, J. B., Dudhia, J., Gill, D. O., Barker, D. M., Duda, M. G., Huang, X., Wang, W., and Powers, J. G.: A description of the advanced research WRF version 3, NCAR Tech. Note NCAR/TN–475+STR, Natl. Cent. for Atmos. Res., Boulder, Colorado, 8 pp., 2008.
- Song, J., Xia, X., Che, H., Wang, J., Zhang, X., and Li, X.: Daytime variation of aerosol optical depth in North China and its impact on aerosol direct radiative effects, *Atmos. Environ.*, 182, 31–40, <https://doi.org/10.1016/j.atmosenv.2018.03.024>, 2018.
- Stauffer, D. R. and Seaman, N. L.: Use of four-dimensional data assimilation in a limited-area mesoscale model, Part I: Experiments with synoptic-scale data, *Mon. Weather Rev.*, 118, 1250–1277, 1990.
- Su, T., Li, Z., and Kahn, R.: Relationships between the planetary boundary layer height and surface pollutants derived from lidar observations over China: regional pattern and influencing factors, *Atmos. Chem. Phys.*, 18, 15921–15935, <https://doi.org/10.5194/acp-18-15921-2018>, 2018.
- Sun, Y. L., Wang, Z. F., Du, W., Zhang, Q., Wang, Q. Q., Fu, P. Q., Pan, X. L., Li, J., Jayne, J., and Worsnop, D. R.: Long-term real-time measurements of aerosol particle composition in Beijing, China: seasonal variations, meteorological effects, and source analysis, *Atmos. Chem. Phys.*, 15, 10149–10165, <https://doi.org/10.5194/acp-15-10149-2015>, 2015.
- Tao, M., Chen, L., Li, R., Wang, L., Wang, J., Wang, Z., Tang, G., and Tao, J.: Spatial oscillation of the particle pollution in eastern China during winter: Implications for re-

- gional air quality and climate, *Atmos. Environ.*, 144, 100–110, <https://doi.org/10.1016/j.atmosenv.2016.08.049>, 2016.
- Tao, W., Liu, J., Ban-Weiss, G. A., Hauglustaine, D. A., Zhang, L., Zhang, Q., Cheng, Y., Yu, Y., and Tao, S.: Effects of urban land expansion on the regional meteorology and air quality of eastern China, *Atmos. Chem. Phys.*, 15, 8597–8614, <https://doi.org/10.5194/acp-15-8597-2015>, 2015.
- Tiwari, S., Srivastava, A. K., Bisht, D. S., Parmita, P., Srivastava, M. K., and Attri, S. D.: Diurnal and seasonal variations of black carbon and PM_{2.5} over New Delhi, India: Influence of meteorology, *Atmos. Res.*, 125–126, 50–62, <https://doi.org/10.1016/j.atmosres.2013.01.011>, 2013.
- University of Science and Technology of China: Resource list, available at: <http://aemol.ustc.edu.cn/product/list/>, last access: 5 March 2020.
- Wang, G., Zhang, R., Gomez, M. E., Yang, L., Levy Zamora, M., Hu, M., Lin, Y., Peng, J., Guo, S., Meng, J., Li, J., Cheng, C., Hu, T., Ren, Y., Wang, Y., Gao, J., Cao, J., An, Z., Zhou, W., Li, G., Wang, J., Tian, P., Marrero-Ortiz, W., Secrest, J., Du, Z., Zheng, J., Shang, D., Zeng, L., Shao, M., Wang, W., Huang, Y., Wang, Y., Zhu, Y., Li, Y., Hu, J., Pan, B., Cai, L., Cheng, Y., Ji, Y., Zhang, F., Rosenfeld, D., Liss, P. S., Duce, R. A., Kolb, C. E., and Molina, M. J.: Persistent sulfate formation from London Fog to Chinese haze, *P. Natl. Acad. Sci. USA*, 113, 13630–13635, <https://doi.org/10.1073/pnas.1616540113>, 2016.
- Wang, J., Christopher, S. A., Nair, U. S., Reid, J. S., Prins, E. M., Szykman, J., and Hand, J. L.: Mesoscale modeling of Central American smoke transport to the United States: 1. “Top-down” assessment of emission strength and diurnal variation impacts, *J. Geophys. Res.-Atmos.*, 111, D05S17, <https://doi.org/10.1029/2005JD006416>, 2006.
- Wang, X., Liang, X.-Z., Jiang, W., Tao, Z., Wang, J. X. L., Liu, H., Han, Z., Liu, S., Zhang, Y., and Grell, G. A.: WRF-Chem simulation of East Asian air quality: Sensitivity to temporal and vertical emissions distributions, *Atmos. Environ.*, 44, 660–669, <https://doi.org/10.1016/j.atmosenv.2009.11.011>, 2010.
- Wang, X.P., Mauzerall, D. L., Hu, Y., Russell, A. G., Larson, E. D., Woo, J.-H., Streets, D. G., and Guenther, A.: A high-resolution emission inventory for eastern China in 2000 and three scenarios for 2020, *Atmos. Environ.*, 39, 5917–5933, <https://doi.org/10.1016/j.atmosenv.2005.06.051>, 2005.
- Wang, Y. G., Ying, Q., Hu, J., and Zhang, H.: Spatial and temporal variations of six criteria air pollutants in 31 provincial capital cities in China during 2013–2014, *Environ. Int.*, 73, 413–422, <https://doi.org/10.1016/j.envint.2014.08.016>, 2014.
- Wang, Y.J., Li, L., Chen, C., Huang, C., Huang, H., Feng, J., Wang, S., Wang, H., Zhang, G., Zhou, M., Cheng, P., Wu, M., Sheng, G., Fu, J., Hu, Y., Russell, A. G., and Wumaer, A.: Source apportionment of fine particulate matter during autumn haze episodes in Shanghai, China, *J. Geophys. Res.-Atmos.*, 119, 1903–1914, <https://doi.org/10.1002/2013JD019630>, 2014.
- Wang, Y.X., Zhang, Q., Jiang, J., Zhou, W., Wang, B., He, K., Duan, F., Zhang, Q., Philip, S., and Xie, Y.: Enhanced sulfate formation during China’s severe winter haze episode in January 2013 missing from current models, *J. Geophys. Res.-Atmos.*, 119, 10425–10440, <https://doi.org/10.1002/2013JD021426>, 2014.
- Wang, Z., Liu, D., Wang, Y., and Shi, G.: Diurnal aerosol variations do affect daily averaged radiative forcing under heavy aerosol loading observed in Hefei, China, *Atmos. Meas. Tech.*, 8, 2901–2907, <https://doi.org/10.5194/amt-8-2901-2015>, 2015.
- Wang, Z.F., Li, J., Wang, Z., Yang, W., Tang, X., Ge, B., Yan, P., Zhu, L., Chen, X., Chen, H., Wand, W., Li, J., Liu, B., Wang, X., Zhao, Y., Lu, N., and Su, D.: Modeling study of regional severe hazes over mid-eastern China in January 2013 and its implications on pollution prevention and control, *Sci. China Earth Sci.*, 57, 3–13, <https://doi.org/10.1007/s11430-013-4793-0>, 2014.
- Wiedinmyer, C., Akagi, S. K., Yokelson, R. J., Emmons, L. K., Al-Saadi, J. A., Orlando, J. J., and Soja, A. J.: The Fire INventory from NCAR (FINN): a high resolution global model to estimate the emissions from open burning, *Geosci. Model Dev.*, 4, 625–641, <https://doi.org/10.5194/gmd-4-625-2011>, 2011.
- Woo, J. H., Baek, J. M., Kim, J. W., Carmichael, G. R., Thongboonchoo, N., Kim, S. T., and An, J. H.: Development of a multi-resolution emission inventory and its impact on sulfur distribution for Northeast Asia, *Water Air Soil Poll.*, 148, 259–278, <https://doi.org/10.1023/A:1025493321901>, 2003.
- WRAP – Western Regional Air Partnership: 2002 Fire Emission Inventory for the WRAP Region – Phase II, Project No. 178-6, available at: <http://www.wrapair.org/forums/fejftasks/FEJFtask7PhaseII.html> (last access: 2 January 2020), 22 July 2005.
- WRF: WRF Source Codes and Graphics Software Downloads, available at: http://www2.mmm.ucar.edu/wrf/users/download/get_source.html, last access: 5 March 2020.
- Wu, L., Su, H., and Jiang, J. H.: Regional simulation of aerosol impacts on precipitation during the East Asian summer monsoon, *J. Geophys. Res.-Atmos.*, 118, 6454–6467, <https://doi.org/10.1002/jgrd.50527>, 2013.
- Xie, Y., Zhao, B., Zhang, L., and Luo, R.: Spatiotemporal variations of PM_{2.5} and PM₁₀ concentrations between 31 Chinese cities and their relationships with SO₂, NO₂, CO and O₃, *Particuology*, 20, 141–149, <https://doi.org/10.1016/j.partic.2015.01.003>, 2015.
- Xu, W., Sun, Y., Wang, Q., Zhao, J., Wang, J., Ge, X., Xie, C., Zhou, W., Du, W., Li, J., Fu, P., Wang, Z., Worsnop, D. R., and Coe, H.: Changes in Aerosol Chemistry From 2014 to 2016 in Winter in Beijing: Insights From High-Resolution Aerosol Mass Spectrometry, *J. Geophys. Res.-Atmos.*, 124, 1132–1147, <https://doi.org/10.1029/2018JD029245>, 2019.
- Xu, W. Y., Zhao, C. S., Ran, L., Lin, W. L., Yan, P., and Xu, X. B.: SO₂ noontime-peak phenomenon in the North China Plain, *Atmos. Chem. Phys.*, 14, 7757–7768, <https://doi.org/10.5194/acp-14-7757-2014>, 2014.
- Yang, Y., Liao, H., and Lou, S.: Increase in winter haze over eastern China in recent decades: Roles of variations in meteorological parameters and anthropogenic emissions, *J. Geophys. Res.-Atmos.*, 121, 13050–13065, 2016.
- Yang, Y., Smith, S. J., Wang, H., Lou, S., and Rasch, P. J.: Impact of Anthropogenic Emission Injection Height Uncertainty on Global Sulfur Dioxide and Aerosol Distribution, *J. Geophys. Res.-Atmos.*, 124, 4812–4826, <https://doi.org/10.1029/2018JD030001>, 2019.
- Ying, Z., Tie, X., and Li, G.: Sensitivity of ozone concentrations to diurnal variations of surface emissions in Mexico City: A WRF/Chem modeling study, *Atmos. Environ.*, 43, 851–859, <https://doi.org/10.1016/j.atmosenv.2008.10.044>, 2009.
- Zaveri, R. A. and Peters, L. K.: A new lumped structure photochemical mechanism for large-scale applications, *J. Geophys. Res.*,

- 104, 30387–30415, <https://doi.org/10.1029/1999JD900876>, 1999.
- Zaveri, R. A., Easter, R. C., Fast, J. D., and Peters, L. K.: Model for simulating aerosol interactions and chemistry (MOSAIC), *J. Geophys. Res.-Atmos.*, 113, 1–29, <https://doi.org/10.1029/2007JD008782>, 2008.
- Zhang, B., Wang, Y., and Hao, J.: Simulating aerosol–radiation–cloud feedbacks on meteorology and air quality over eastern China under severe haze conditions in winter, *Atmos. Chem. Phys.*, 15, 2387–2404, <https://doi.org/10.5194/acp-15-2387-2015>, 2015.
- Zhang, H., Wang, Y., Hu, J., Ying, Q., and Hu, X.-M.: Relationships between meteorological parameters and criteria air pollutants in three megacities in China, *Environ. Res.*, 140, 242–254, <https://doi.org/10.1016/j.envres.2015.04.004>, 2015.
- Zhang, L., Liao, H., and Li, J.: Impacts of Asian summer monsoon on seasonal and interannual variations of aerosols over eastern China, *J. Geophys. Res.*, 115, D10307, <https://doi.org/10.1029/2009JD012299>, 2010.
- Zhang, L., Wang, T., Lv, M., and Zhang, Q.: On the severe haze in Beijing during January 2013: Unraveling the effects of meteorological anomalies with WRF-Chem, *Atmos. Environ.*, 104, 11–21, <https://doi.org/10.1016/j.atmosenv.2015.01.001>, 2015.
- Zhang, Y., Zhang, X., Wang, L., Zhang, Q., Duan, F., and He, K.: Application of WRF/Chem over East Asia: Part I. Model evaluation and intercomparison with MM5/CMAQ, *Atmos. Environ.*, 124, 285–300, <https://doi.org/10.1016/j.atmosenv.2015.07.022>, 2016.
- Zhang, Y.-L. and Cao, F.: Fine particulate matter (PM_{2.5}) in China at a city level, *Scient. Rep.*, 5, 14884, <https://doi.org/10.1038/srep14884>, 2015.
- Zhao, B., Liou, K.-N., Gu, Y., Li, Q., Jiang, J. H., Su, H., He, C., Tseng, H.-L. R., Wang, S., Liu, R., Qi, L., Lee, W.-L., and Hao, J.: Enhanced PM_{2.5} pollution in China due to aerosol–cloud interactions, *Scient. Rep.*, 7, 4453, <https://doi.org/10.1038/s41598-017-04096-8>, 2017.
- Zhao, C., Liu, X., Leung, L. R., Johnson, B., McFarlane, S. A., Gustafson Jr., W. I., Fast, J. D., and Easter, R.: The spatial distribution of mineral dust and its shortwave radiative forcing over North Africa: modeling sensitivities to dust emissions and aerosol size treatments, *Atmos. Chem. Phys.*, 10, 8821–8838, <https://doi.org/10.5194/acp-10-8821-2010>, 2010.
- Zhao, C., Liu, X., Ruby Leung, L., and Hagos, S.: Radiative impact of mineral dust on monsoon precipitation variability over West Africa, *Atmos. Chem. Phys.*, 11, 1879–1893, <https://doi.org/10.5194/acp-11-1879-2011>, 2011.
- Zhao, C., Liu, X., and Leung, L. R.: Impact of the Desert dust on the summer monsoon system over Southwestern North America, *Atmos. Chem. Phys.*, 12, 3717–3731, <https://doi.org/10.5194/acp-12-3717-2012>, 2012.
- Zhao, C., Chen, S., Leung, L. R., Qian, Y., Kok, J. F., Zaveri, R. A., and Huang, J.: Uncertainty in modeling dust mass balance and radiative forcing from size parameterization, *Atmos. Chem. Phys.*, 13, 10733–10753, <https://doi.org/10.5194/acp-13-10733-2013>, 2013a.
- Zhao, C., Ruby Leung, L., Easter, R., Hand, J., and Avise, J.: Characterization of speciated aerosol direct radiative forcing over California, *J. Geophys. Res.-Atmos.*, 118, 2372–2388, <https://doi.org/10.1029/2012JD018364>, 2013b.
- Zhao, C., Hu, Z., Qian, Y., Ruby Leung, L., Huang, M., Jin, J., Flanner, M. G., Zhang, R., Wang, H., Yan, H., Lu, Z., and Streets, D. G.: Simulating black carbon and dust and their radiative forcing in seasonal snow: a case study over North China with field campaign measurements, *Atmos. Chem. Phys.*, 14, 11475–11491, <https://doi.org/10.5194/acp-14-11475-2014>, 2014.
- Zhao, C., Huang, M., Fast, J. D., Berg, L. K., Qian, Y., Guenther, A., Gu, D., Shrivastava, M., Liu, Y., Walters, S., Pfister, G., Jin, J., Shilling, J. E., and Warneke, C.: Sensitivity of biogenic volatile organic compounds to land surface parameterizations and vegetation distributions in California, *Geosci. Model Dev.*, 9, 1959–1976, <https://doi.org/10.5194/gmd-9-1959-2016>, 2016.
- Zhao, S., Yu, Y., Yin, D., He, J., Liu, N., Qu, J., and Xiao, J.: Annual and diurnal variations of gaseous and particulate pollutants in 31 provincial capital cities based on in situ air quality monitoring data from China National Environmental Monitoring Center, *Environ. Int.*, 86, 92–106, <https://doi.org/10.1016/j.envint.2015.11.003>, 2016.
- Zhong, M., Saikawa, E., Liu, Y., Naik, V., Horowitz, L. W., Takigawa, M., Zhao, Y., Lin, N.-H., and Stone, E. A.: Air quality modeling with WRF-Chem v3.5 in East Asia: sensitivity to emissions and evaluation of simulated air quality, *Geosci. Model Dev.*, 9, 1201–1218, <https://doi.org/10.5194/gmd-9-1201-2016>, 2016.
- Zhou, G., Yang, F., Geng, F., Xu, J., Yang, X., and Tie, X.: Measuring and modeling aerosol: relationship with haze events in Shanghai, China, *Aerosol Air Qual. Res.*, 14, 783–792, 2014.
- Zhou, G., Xu, J., Xie, Y., Chang, L., Gao, W., Gu, Y., and Zhou, J.: Numerical air quality forecasting over eastern China: An operational application of WRF-Chem, *Atmos. Environ.*, 153, 94–108, <https://doi.org/10.1016/j.atmosenv.2017.01.020>, 2017.